Theoretical Study of the Oxidative Addition of Ammonia to Various Unsaturated Low-Valent Transition Metal Species

Stuart A. Macgregor

Department of Chemistry, Heriot-Watt University, Riccarton, Edinburgh, EH14 4AS, U.K.

Received January 22, 2001

Reaction profiles for the oxidative addition of NH_3 to a number of unsaturated low-valent transition metal complexes have been computed using gradient-corrected density functional theory. The metal complexes studied are d^8 CpM(CO) (M = Rh, Ir) and *trans*-$M(PH_3)_2X$ (M = Rh, Ir; X = H, Cl) and d^{10} ML_2 (M = Pd, Pt; L = PH_3, $L_2 = H_2PCH_2CH_2PH_2$, dpe). Reactions with the d^8 species are characterized by the formation of strongly bound ammine complexes from which computed activation energies for oxidative addition are in excess of 16 kcal mol^{-1}. Computed reaction enthalpies are all exothermic with these complexes. With d^{10} $M(PH_3)_2$ species computed ammine adducts are weak, activation barriers are in excess of 23 kcal mol^{-1}, and the overall reaction is endothermic for both M = Pd and Pt. The introduction of the chelating dpe ligand results in stronger ammine adducts but only slightly reduced computed activation barriers. Of the d^{10} species only the reaction with Pt(dpe) is computed to be exothermic. Comparison of the computed reaction profiles for analogous second- and third-row complexes shows the NH_3 oxidative addition reaction to be more favorable with the third-row species, which exhibit more strongly bound ammine adducts, lower activation barriers, and more exothermic reactions. Of the species studied the most promising unsaturated fragments for effecting NH_3 oxidative addition are CpIr(CO), *trans*-$Ir(PH_3)_2X$ (X = H, Cl), and Pt(dpe). The more favorable thermodynamics computed with these third-row species arise from higher M−NH_2 and M−H homolytic bond strengths in the hydrido-amido products. M-NH_2 bonds are computed to be between 6 and 13 kcal mol^{-1} and M−H bonds between 5 and 14 kcal mol^{-1} stronger in the third-row complexes compared to their second-row congeners. For complexes exhibiting no N→M π-donation M−NH_2 bonds are computed to be up to 26 kcal mol^{-1} weaker than M−H bonds. N→M π-donation reduces this differential, and in $Ir(PH_3)_2(H)_2(NH_2)$ the Ir−NH_2 and Ir−H bonds are calculated to have equal homolytic bond strengths. Computed activation energies for NH_3 oxidative addition do not appear to be related to the strength of the ammine adduct, and for metal complexes of the same row the computed activation energy is relatively insensitive to the nature of the unsaturated fragment. These findings are discussed in terms of an NH_3 reorientation/N−H bond activation model for the oxidative addition reaction. Although strongly Lewis acidic metal fragments usually promote oxidative addition, with NH_3 these form strong ammine adducts from which NH_3 reorientation is energetically costly. For metal fragments with lower Lewis acidity NH_3 reorientation is more facile, but the subsequent oxidative addition remains difficult. These ideas are supported by the accessibility of η^1-H and η^3-H,H,H NH_3 adducts formed with Pt(dpe), while with $Ir(PH_3)_2Cl$ only a high-energy η^1-H species was located.

Introduction

Low-valent transition metal amides are of current interest due to their role as intermediates in catalytic schemes for alkene hydroamination,[1,2] aryl amination,[3] and imine hydrogenation.[4] The synthesis of low-valent transition metal amides as models for such intermediates has therefore received increased attention, and a well-defined reaction chemistry of low-valent metal amides analogous to that of traditional organometallic species has begun to emerge.[5] Examples of this "inorganometallic" chemistry include the insertion reactions of CO,[6] activated alkenes,[7] or alkynes[8] into low-valent metal−amide bonds, β-H elimination,[6c,9] and C−N bond forming reductive elimination. [3,10]

A variety of synthetic routes to low-valent transition metal amides have now been developed.[5] Methods

(1) (a) Müller, T. E.; Beller, M. *Chem.* Rev. **1998**, 98, 675. (b) Brunet, J.-J. *Gazz. Chim. Ital.* **1997**, *127*, 111. (c) Taube, R. In *Applied Homogeneous Catalysis with Organometallic Compounds*; Cornils, B.; Herrmann, W. A., Eds., VCH: Weinheim; 1996; p 507. (d) Roundhill, D. M. *Chem. Rev.* **1992**, *92*, 1.

(2) Beller and co-workers have published a series of articles on the oxidative amination of aromatic alkenes to enamines: (a) Beller, M.; Trauthwein, H.; Eichberger, M.; Breindl, C.; Herwig, J.; Müller, T. E.; Thiel, O. R. *Chem. Eur. J.* **1999**, *5*, 1306. (b) Beller, M.; Trauthwein, H.; Eichberger, M.; Breindl, C.; Müller, T. E. *Eur. J. Inorg. Chem.* **1999**, 1121. (c) Beller, M.; Trauthwein, H.; Eichberger, M.; Breindl, C.; Müller, T. E.; Zapf, A. *J. Organomet. Chem.* **1998**, *566*, 277. (d) Beller, M.; Eichberger, M.; Trauthwein, H. *Angew. Chem., Int. Ed. Engl.* **1997**, *36*, 2225.

10.1021/om010044w CCC: $20.00
Publication on Web 03/30/2001

include deprotonation of metal amine complexes,[6c,11] proton exchange reactions between free amines and metal hydroxides or alkoxides,[12] halide metathesis reactions with alkali metal amides,[10b,13] and the treatment of metal alkyls with organoazides.[10c] The use of an NH_2^-/NH_3 base/conjugate acid metathesis approach for the syntheses of *trans*-Ru(dmpe)$_2$(H)(NH_2) and Cp*Ir(PMe_3)(Ph)(NH_2) has recently been reported.[14]

In principle, an additional method of introducing an amide moiety to a metal center would be through the direct oxidative addition of an N−H bond of ammonia or a primary or secondary amine. The formal oxidative addition of activated N−H bonds is well known.[15] However, these reactions appear to depend on the presence of relatively acidic N−H bonds and may often proceed via initial protonation of the metal center rather than a direct oxidative addition process. For example, [Pt(PCy_3)$_2$] was found to activate the more acidic N−H bonds of pyrrole and pentafluoroaniline but not those of aniline.[16] Similarly, the rate of amide N−H bond activation by Ru(dmpe)$_2$(H)(naphthyl) was found to be dependent on amide acidity and, for $F_3CC(O)NH_2$, occurred at a rate faster than reductive elimination of naphthalene. This rules out, in this case, a reductive elimination/N−H bond activation pathway.[17]

The activation of primary and secondary amine as well as ammonia N−H bonds by low-valent transition metal centers has been achieved however.[18,19] The first example of the oxidative addition of NH_3 by a monomeric late transition metal center was reported by Casalnuovo and co-workers, who isolated a series of bridging-amido dimers from an initial reaction with Ir(PEt_3)$_2$(C_2H_4)$_2$Cl.[20] The active species in this process was thought to be 14-electron Ir(PEt_3)$_2$Cl. Milstein's group has subsequently reported on NH_3 activation at various Ir(I) centers.[21] Several cases of the reverse reaction, N−H bond forming reductive elimination, have also been published.[7,11b,15d,22] These reactions are often prompted by ligand addition, although the formation of pyrrole from Ir(PPh_3)$_2$(CO)(H)$_2$(NC_4H_4) was postulated to occur either directly or via initial irreversible ligand loss.[23]

The oxidative addition of an N−H bond to a low-valent transition metal center is potentially an important step in catalytic schemes for alkene hydroamination. Casalnuovo and co-workers extended their original NH_3 activation chemistry to produce a full catalytic cycle for the hydroamination of norbornene with aniline.[24] Initial oxidative addition of aniline to Ir(PEt_3)$_2$Cl yields a five-coordinate hydrido-amido intermediate to which norbornene can bind and subsequently insert into the iridium−amide bond. Lewis acid-promoted C−H bond forming reductive elimination from the resultant azairidacycle yields the hydroamination product. An analogous catalytic system based on chiral bidentate phosphine ligands has been employed to effect the asymmetric hydroamination of norbornene;[25] however for both these examples the activity of the iridium catalyst is low. Several other examples of hydroamination reactions thought to involve initial N−H activation have been published.[26,27] An alternative hydroamination scheme relies upon the initial activation of the unsaturated substrate at an electron-deficient late transition metal

(3) (a) Wolfe, J. P.; Wagaw, S.; Marcoux, J.-F.; Buchwald, S. L. *Acc. Chem. Res.* **1998**, *31*, 805. (b) Hartwig, J. F. *Synlett* **1997**, 329.

(4) (a) Ohkuma, T.; Kitamura, M.; Noyori, R. In *Catalytic Asymmetric Synthesis*, 2nd ed.; Ojima, I., Ed.; Wiley-VCH: New York, 2000. (b) Becalski, A. G.; Cullen, W. R.; Fryzuk, M. D.; James, B. R.; Kang, G.-J.; Rettig, S. J. *Inorg. Chem.* **1991**, *30*, 5002. (c) Fryzuk, M. D.; Piers, W. E. *Organometallics* **1990**, *9*, 986. (d) Longley, C. J.; Goodwin, T. J.; Wilkinson, G. *Polyhedron* **1986**, *5*, 1625.

(5) (a) Fryzuk, M. D.; Montgomery, C. D. *Coord. Chem. Rev.* **1989**, *95*, 1. (b) Bryndza, H. E.; Tam, W. *Chem. Rev.* **1988**, *88*, 1163.

(6) (a) Holland, P. L.; Andersen, R. A.; Bergman, R. G. *J. Am. Chem. Soc.* **1996**, *118*, 1092. (b) Rahim, M.; Bushweller, C. H.; Ahmed, K. J. *Organometallics* **1994**, *13*, 4952. (c) Joslin, F. L.; Johnson, M. P.; Mague, J. T.; Roundhill, D. M. *Organometallics* **1991**, *10*, 2781. (d) Bryndza, H. E.; Fultz, W. C.; Tam, W. *Organometallics* **1985**, *4*, 939.

(7) (a) Cowan, R. L.; Trogler, W. C. *J. Am. Chem. Soc.* **1989**, *111*, 4750. (b) Cowan, R. L.; Trogler, W. C. *Organometallics* **1987**, *6*, 2451.

(8) (a) Boncella, J. M.; Eve, T. M.; Rickman, B.; Abboud, K. A. *Polyhedron* **1998**, *17*, 725. (b) Villanueva, L. A.; Abboud, K. A.; Boncella, J. M. *Organometallics* **1992**, *11*, 2963.

(9) (a) Hartwig, J. F. *J. Am. Chem. Soc.* **1996**, *118*, 7010. (b) Diamond, S. E.; Mares, F. *J. Organomet. Chem.* **1977**, *142*, C55.

(10) (a) Hartwig, J. F. *Angew. Chem., Int. Engl.* **1998**, *37*, 2046. (b) Driver, M. S.; Hartwig, J. F. *J. Am. Chem. Soc.* **1997**, *119*, 8232. (c) Koo, K.; Hillhouse, G. L. *Organometallics* **1996**, *15*, 2669. (d) Villanueva, L. A.; Abboud, K. A.; Boncella, J. M. *Organometallics* **1994**, *13*, 3921.

(11) (a) Dewey, M. A.; Knight, D. A.; Arif, A.; Gladysz, J. A. *Chem. Ber.* **1992**, *125*, 815. (b) Park, S.; Rheingold, A. L.; Roundhill, D. M. *Organometallics* **1991**, *10*, 615.

(12) (a) Li, J. J.; Li, W.; James, A. J.; Holbert, T.; Sharp, T. P.; Sharp, P. R. *Inorg. Chem.* **1999**, *38*, 1563. (b) Ruiz, J.; Rodríquez, V.; López, G.; Chaloner, P. A.; Hitchcock, P. B. *J. Chem. Soc., Dalton Trans.* **1997**, 4271. (c) Driver, M. S.; Hartwig, J. F. *Organometallics* **1997**, *16*, 5706. (d) Glueck, D. S.; Winslow, L. J. N.; Bergman, R. G. *Organometallics* **1991**, *10*, 1462.

(13) (a) Brunet, J.-J.; Daran, J.-C.; Neibecker, D.; Rosenberg, L. *J. Organomet. Chem.* **1997**, *538*, 251. (b) VanderLende, D. D.; Abboud, K. A.; Boncella, J. M. *Inorg. Chem.* **1995**, *34*, 5319. (c) Kim, Y-J.; Choi, J.-C.; Osakada, K. *J. Organomet. Chem.* **1995**, *491*, 97.

(14) Kaplan, A. W.; Ritter, J. C. M.; Bergman, R. G. *J. Am. Chem. Soc.* **1998**, *120*, 6828.

(15) For example, heterocyclic NH bonds: (a) Dubuc, I.; Dubois, M.-A.; Bélanger-Gariépy, F.; Zargarian, D. *Organometallics* **1999**, *18*, 30. (b) Jones, W. D.; Dong, L.; Myers, A. W. *Organometallics* **1995**, *14*, 855. (c) Lapido, F. T.; Merola, J. S. *Inorg. Chem.* **1990**, *29*, 4172. (d) Yamamoto, T.; Sano, K.; Yamamoto, A. *Chem. Lett.* **1982**, 907. (e) Roundhill, D. M. *Inorg. Chem.* **1970**, *9*, 254. (f) Nelson, J. H.; Schmitt, D. L.; Henry, R. A.; Moore, D. W.; Jonassen, H. B. *Inorg. Chem.* **1970**, *9*, 2678. Ammonium cations: (g) Goel, R. G.; Srivastava, R. C. *J. Organomet. Chem.* **1983**, *244*, 303. (h) Rauchfuss, T. B.; Roundhill, D. M. *J. Am. Chem. Soc.* **1974**, *96*, 3098. (i) Mague, J. T. *Inorg. Chem.* **1972**, *11*, 2558. Amidines: (j) Clark, T.; Robinson, S. D. *J. Chem. Soc., Dalton Trans.* **1993**, 2827. Amides: (k) Hursthouse, M. B.; Mazid, M. A.; Robinson, S. D.; Sahajpal, A. *J. Chem. Soc., Dalton Trans.* **1993**, 2835. (l) Schaad, D. R.; Landis, C. R. *Organometallics* **1992**, *11*, 2024.

(16) Fornies, J.; Green, M.; Spencer, J. L.; Stone, F. G. A. *J. Chem. Soc., Dalton Trans.* **1977**, 1006.

(17) Schaad, D. R.; Landis, C. R. *J. Am. Chem. Soc.* **1990**, *112*, 1628.

(18) For examples involving cluster compounds see: (a) Bryan, E. G.; Johnson, B. F. G.; Lewis, J. *J. Chem. Soc., Dalton Trans.* **1977**, 1328. (b) Sappa, E.; Milone, L. *J. Organomet. Chem.* **1973**, *61*, 383.

(19) For the "chelate-assisted" oxidative addition of pendant amine N−H bonds see: Park, S.; Johnson, M. P.; Roundhill, D. M. *Organometallics* **1989**, *8*, 1700, and references therein.

(20) Casalnuovo, A. L.; Calabrese, J. C.; Milstein, D. *Inorg. Chem.* **1987**, *26*, 971.

(21) (a) Koelliker, R.; Milstein, D. *J. Am. Chem. Soc.* **1991**, *113*, 8524. (b) Koelliker, R.; Milstein, D. *Angew. Chem., Int. Ed. Engl.* **1991**, *30*, 707. (c) Schulz, M.; Milstein, D. *J. Chem. Soc., Chem. Commun.* **1993**, 318.

(22) (a) Glueck, D. S.; Winslow, L. J. N.; Bergman, R. G. *Organometallics* **1991**, *10*, 1462. (b) Hartwig, J. F.; Andersen, R. A.; Bergman, R. G. *Organometallics* **1991**, *10*, 1875. (c) Segilson, A. L.; Cowan, R. L.; Trogler, W. C. *Inorg. Chem.* **1991**, *30*, 3371.

(23) Driver, M. S.; Hartwig, J. F. *Organometallics* **1998**, *17*, 1134.

(24) Casalnuovo, A. L.; Calabrese, J. C.; Milstein, D. *J. Am. Chem. Soc.* **1988**, *110*, 6738.

(25) Dorta, R.; Egli, P.; Zürcher, F.; Togni, A. *J. Am. Chem. Soc.* **1997**, *119*, 10857.

(26) (a) Beller, M.; Trauthwein, H.; Eichberger, M.; Breindl, C.; Herwig, J.; Müller, T. E.; Thiel, O. R. *Eur. J. Chem.* **1999**, *5*, 1306. (b) Uchimaru, Y. *J. Chem. Soc., Chem. Commun.* **1999**, 1133. (c) Nakamura, I.; Itagaki, H.; Yamamoto, Y. *J. Org. Chem.* **1998**, *63*, 6458. (d) Diversi, P.; Ermini, L.; Ingrosso, G.; Lucherini, A.; Pinzino, C.; Sagramora, L. *J. Organomet. Chem.* **1995**, *494*, C1. (e) Brunet, J.-J.; Commenges, G.; Neibecker, D.; Philippot, K. *J. Organomet. Chem.* **1994**, *469*, 221. (f) Baig, T.; Jenck, J.; Kalck, P. *J. Chem. Soc., Chem. Commun.* **1992**, 1552.

center. C−N bond formation can then occur via nucleophilic attack by an amine at the bound alkene. Stoichiometric hydroaminations based on this approach have been developed as well as a number of catalytic processes.[1,28] However, thus far catalysis has been limited to the more favorable intramolecular cyclization of amino-alkenes[29] or -alkynes[30] or has only proved successful with activated alkenes.[31] To date, therefore, a general catalytic procedure for the hydroamination of alkenes has yet to be achieved.

It is against this background that the present density functional computational study focusing on the oxidative addition of NH_3 to unsaturated low-valent transition metal complexes, a key step in hydroamination schemes based on N−H bond activation, has been undertaken. The metal species studied are CpM(CO)[32] (M = Rh, Ir), *trans*-$M(PH_3)_2X$[33] (M = Rh, Ir; X = Cl, H: hereafter the *trans* isomer will be assumed unless otherwise stated), and ML_2[34] (M = Pd, Pt; L = PH_3; L_2 = $H_2PCH_2CH_2PH_2$, diphosphinoethane or dpe). While numerous theoretical studies on the oxidative addition of simple substrate molecules to the unsaturated metal species employed in this study have been published,[32−35] only two theoretical studies of the oxidative addition of NH_3 have appeared. Siegbahn and co-workers computed profiles for the oxidative addition of NH_3 to second-row transition metal atoms.[36] They found the reaction to be most exothermic and to have minimal activation barriers for the early transition metals (Y to Nb). Of the later transition metals the reaction with rhodium was most favorable and entailed the lowest activation barrier. For rhodium and palladium atoms the energetics of the oxidative addition reactions with NH_3 and CH_4 were calculated to be very similar. Musaev and Morokuma have compared the activation of R−H bonds by the CpRh(CO) fragment (R = H, CH_3, NH_2, OH, SiH_3).[32c] They found both the activation barrier and the reaction exothermicity to be related to the strength of the cleaving R−H and forming Rh−R bonds. Thus the oxidative additions of H_2 and SiH_4 do not entail a barrier, while for CH_4 a weakly bound precursor complex is located from which oxidative addition proceeds with an activation energy of 6 kcal mol^{-1}. Relative to the isolated reactants all three reactions are computed to be strongly exothermic (−49.4, −31.0, and −16.4 kcal mol^{-1} for R = SiH_3, H, and CH_3 respectively). The oxidative additions of NH_3 and H_2O are far less favored, in part due to the stronger H−OH and H−NH_2 bonds to be cleaved and the weaker Rh−NH_2 and Rh−OH bonds that are formed However in these cases a very stable precursor ammine or aquo complex is formed from which activation barriers are computed to be large (42 and 26 kcal mol^{-1} for NH_3 and H_2O, respectively). These processes are computed, relative to the isolated reactants, to be only slightly exothermic (−2.4 and −3.2 kcal mol^{-1} for R = OH and NH_2, respectively). Compared to the calculations involving activation by transition metal atoms,[36] this study shows the energetics of CH_4 and NH_3 oxidative addition to diverge sharply when activation is by a molecular species.

Very recently, Senn et al. have employed molecular dynamics DFT calculations to study the hydroamination of ethene at $[MCl(PH_3)_2(C_2H_4)]^{z+}$ metal complexes (M = Co, Rh, Ir, z = 0; M = Ni, Pd, Pt, z = 1) based on external nucleophilic attack of NH_3 at the bound alkene.[37] For group 9 metals NH_3 nucleophilic addition was found to be the rate-determining step, while for group 10 metals cleavage of the β-aminoalkyl M−C bond was rate limiting. Overall the Ni complex was found to be most promising for catalysis, with an activation barrier for the rate-determining step of 108 kJ mol^{-1}.

The aim of the present work will be to survey the ability of a variety of unsaturated transition metal fragments to effect the oxidative addition of NH_3 via a concerted N−H bond addition mechanism. The role of the metal center (second vs third row) and the nature of the auxiliary ligands in promoting this process will be assessed and related to the strength of the new metal−amide and −hydride bonds formed and the details of the oxidative addition process.

Computational Details

All calculations used the Amsterdam Density Functional program ADF1999.[38] A triple-ζ-STO basis set was employed for all metal atoms. All hydride ligands and N-bound hydrogens were described by a triple-ζ plus polarization STO basis set, and a double-ζ plus polarization STO basis set was used for all other atoms. The frozen core approximation was employed with the 1s electrons of C, N, and O atoms, up to

(27) Intermolecular amination of alkenes and alkynes based on initial amine activation has been achieved using early transition metal, lanthanide, or actinide complexes: (a) Li, Y.; Marks, T. J. *Organometallics* **1996**, *15*, 3770. (b) Haskel, A.; Straub, T.; Eisen, M. S. *Organometallics* **1996**, *15*, 3773. (c) Walsh, P. J.; Hollander, F. J.; Bergman, R. G. *Organometallics* **1993**, *12*, 3705.

(28) Hegedus, L. S. *Angew. Chem., Int. Ed. Engl.* **1988**, *27*, 1113, and references therein.

(29) (a) Larock, R. C.; Hightower, T. R.; Hasvold, L. A.; Peterson, K. P. *J. Org. Chem.* **1996**, *61*, 3584. (b) Hegedus, L. S.; Allen, G. F.; Bozell, J. J.; Waterman, E. L. *J. Am. Chem. Soc.* **1978**, *100*, 5800.

(30) (a) Müller, T. E.; Grosche, M.; Herdtweck, E.; Pleier, A.-K.; Walter, E.; Yan, Y.-K. *Organometallics* **2000**, *19*, 170. (b) Müller, T. E.; Pleier, A.-K. *J. Chem. Soc., Dalton Trans.* **1999**, 583.

(31) Segilson, A. L.; Trogler, W. C. *Organometallics* **1993**, *12*, 744.

(32) For previous theoretical studies on oxidative addition processes involving CpMCO fragments see: (a) Ziegler, T.; Tschinke, V.; Fan, L.; Becke, A. D. *J. Am. Chem. Soc.* **1989**, *111*, 9177. (b) Song, J.; Hall, M. B. *Organometallics* **1993**, *12*, 3118. (c) Musaev, D. G.; Morokuma, K. *J. Am. Chem. Soc.* **1995**, *117*, 799. (d) Siegbahn, P. E. M. *J. Am. Chem. Soc.* **1996**, *118*, 1487. (e) Su, M.-D.; Chu, S.-Y. *Chem. Eur. J.* **1999**, *5*, 198.

(33) For $M(PH_3)_2X$ fragments see: (a) Koga, N.; Morokuma, K. *J. Phys. Chem.* **1990**, *94*, 5454. (b) Blomberg, M. R. A.; Siegbahn, P. E. M.; Svensson, M. *J. Am. Chem. Soc.* **1992**, *114*, 6095. (c) Cundari, T. *J. Am. Chem. Soc.* **1994**, *116*, 340. (d) Margl, P.; Ziegler, T.; Blöchl, P. E. *J. Am. Chem. Soc.* **1995**, *117*, 12625. (e) Rosini, G. P.; Liu, F.; Krogh−Jesperen, K.; Goldman, A. S.; Li, C.; Nolan, S. P. *J. Am. Chem. Soc.* **1998**, *120*, 9256. (f) Su, M.-D.; Chu, S.-Y. *J. Am. Chem. Soc.* **1997**, *119*, 10178. (g) Espinosa-García, J.; Corchado, J. C.; Truhlar, D. C. *J. Am. Chem. Soc.* **1997**, *119*, 9891.

(34) For ML_2 fragments see: (a) Noell, J. O.; Hay, P. J. *J. Am. Chem. Soc.* **1982**, *104*, 4578. (b) Blomberg, M. R. A.; Brandemark, U.; Siegbahn, P. E. M. *J. Am. Chem. Soc.* **1983**, *105*, 5557. (c) Low, J. J.; Goddard, W. A., III. *Organometallics* **1986**, *5*, 609. (d) Low, J. J.; Goddard, W. A., III. *J. Am. Chem. Soc.* **1986**, *108*, 6115. (e) Obara, S.; Kitaura, K.; Morokuma, K. *J. Am. Chem. Soc.* **1984**, *106*, 7482. (f) Matsubara, T.; Maseras, F.; Koga, N.; Morokuma, K. *J. Phys. Chem.* **1996**, *100*, 2573. (g) Sakaki, S.; Biswas, B.; Sugimoto, M. *J. Chem. Soc., Dalton Trans.* **1997**, 803. (h) Sakaki, S.; Biswas, B.; Sugimoto, M. *Organometallics* **1998**, *17*, 1278. (i) Su, M.-D.; Chu, S.-Y. *J. Am. Chem. Soc.* **1997**, *119*, 10178.

(35) For recent reviews see: (a) Nui, S.; Hall, M. B. *Chem. Rev.* **2000**, *100*, 353. (b) Dedieu, A. *Chem. Rev.* **2000**, *100*, 543.

(36) Blomberg, M. R. A.; Siegbahn, P. E. M.; Svensson, M. *Inorg. Chem.* **1993**, *32*, 4218.

(37) Senn, H. M.; Blöchl, P. E.; Togni, A. *J. Am. Chem. Soc.* **2000**, *122*, 4098.

(38) Baerends, E. J.; Ellis, D. E.; Ros, P. *Chem. Phys.* **1973**, *2*, 41. (b) te Velde, G.; Baerends, E. J. *J. Comput. Phys.* **1992**, *99*, 84. (c) Fonseca Guerra, C.; Snijders, J. G.; te Velde, G.; Baerends, E. J. *Theor. Chem. Acc.* **1998**, *99*, 391.

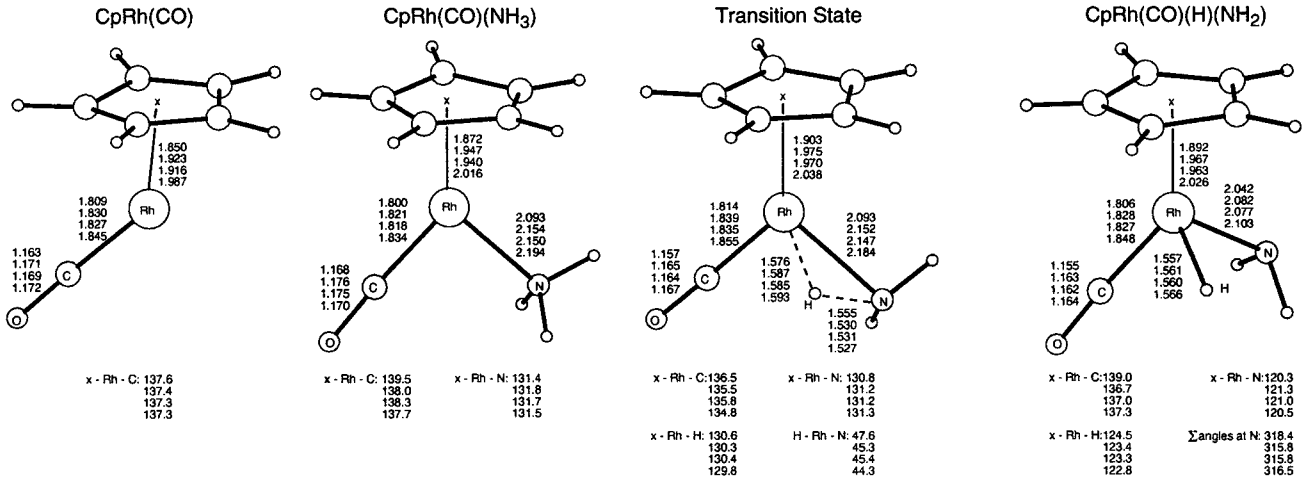

Figure 1. Optimized geometries (Å, deg) for stationary points located for the oxidative addition of NH_3 to CpRh(CO). Data correspond (from the top) to results computed with the LDA, BP, PW91, and BLYP functionals.

and including the 2p of P and Cl, 3d of Rh and Pd, and 4f electrons of Ir and Pt being frozen in calculations. Geometry optimizations were carried out with the gradient corrections due to Becke[39] (exchange) and Perdew[40] (correlation) (denoted BP) included self-consistently in the optimization procedure. All calculations used the optimization procedure developed by Versluis and Ziegler[41] and incorporated the quasi-relativistic corrections of Snijders and co-workers.[42] Geometries were optimized in no higher than C_s or C_2 symmetry as appropriate. All minima at the BP level were characterized using numerical frequency analyses[43] as having no imaginary frequencies, with the exception of some N-bound ammine adduct species, for which single low-energy imaginary modes corresponding to NH_3, PH_3, or Cp ligand rotations were sometimes computed. In some cases reoptimization either in C_1 symmetry or after distortion along the imaginary mode failed to remove these low-energy imaginary frequencies. These calculations indicated, however, that negligible energy changes were associated with these imaginary modes, and therefore energies from the original calculation are reported. Transition states were characterized has having one imaginary frequency.[44] Where two alternative oxidative addition transition state structures were located (pyramidal and planar, see main text), only the lower energy form was characterized in this way. Geometry optimizations following distortion along the unique imaginary mode were then performed to confirm the minima connecting to each transition state structure. In the absence of computed frequencies the expected imaginary mode was simulated by adding ±0.05 Å onto the cleaving N···H distance. Reported energies calculated at the BP level include a correction for zero-point energies unless indicated otherwise. Some results derived from calculations performed at the LDA level (with a subsequent energy correction using the Becke and Perdew gradient corrections, LDA+BP) as well as those in which combinations of gradient corrections due to Becke and Lee, Yang and Parr[45] (BLYP), and Perdew and Wang[46] (PW91) are included self-consistently in the geometry optimizations are also reported. In these cases frequency analyses were not performed as the geometries of all species were found to be analogous to those obtained with BP calculations.

Results

CpM(CO) + NH_3 (M = Rh, Ir). Structures and relative energies of the unsaturated CpM(CO) species, NH_3 adducts, hydrido-amido products, and the transition states for oxidative addition are shown in Figure 1 (M = Rh) and Figure 2 (M = Ir) for calculations performed with the LDA, BP, PW91, and BLYP functionals. The computed CpM(CO) fragment geometries are similar to those found by others, although detailed structures as well as calculated singlet−triplet gaps vary significantly with the computational method employed. With the three gradient-corrected functionals a preference for the singlet form of CpRh(CO) of between 2.0 and 2.7 kcal mol^{-1} was calculated, while triplet CpIr(CO) was found to be between 1.7 and 2.5 kcal mol^{-1} more stable than the corresponding singlet. These results are consistent with earlier studies in that a greater preference for the triplet form is found with M = Ir. As discussed by others, singlet−triplet spin-inversion is expected to be facile for these Ir and Rh complexes.[32] In addition, as the singlet state is likely to be further stabilized by the addition of the ammine ligand, only the singlet species will be considered from now on.[47] The computed geometries in Figures 1 and 2 exhibit, as expected,[48] the shortest metal−ligand bond

(39) Becke, A. D. *Phys. Rev. A* **1988**, *38*, 3098.
(40) Perdew, J. P. *Phys. Rev. B* **1986**, *33*, 8822.
(41) (a) Versluis, L.; Ziegler, T. *J. Chem. Phys.* **1988**, *88*, 322. (b) Fan, L.; Ziegler, T. *J. Am. Chem. Soc.* **1992**, *114*, 10890.
(42) (a) Snijders, J. G.; Baerends, E. J.; Ros, P. *Mol. Phys.* **1979**, *38*, 1909. (b) Ziegler, T.; Tschinke, V.; Baerends, E. J.; Snijders, J. G.; Ravenek, W. *J. Phys. Chem.* **1989**, *93*, 3050. (c) van Lenthe, E.; Baerends, E. J.; Snijders, J. G. *J. Chem. Phys.* **1993**, *99*, 4597.
(43) (a) Fan, L. Ziegler, T. *J. Chem. Phys.* **1992**, *96*, 9005. (b) Fan, L. Ziegler, T. *J. Phys. Chem.* **1992**, *96*, 6937.
(44) The use of the terms "transition state" and "activation energy" in this paper should be clarified. As pointed out by a referee, a stationary point exhibiting one imaginary frequency corresponds strictly speaking to a saddle point on the potential energy surface, rather than a "transition state", the latter being a kinetic concept. Similarly the experimental term "activation energy" includes components due to the barrier height, thermal corrections, and tunneling. Computed activation energies in this paper correspond, when zero-point energy terms are included, to activation enthalpies at 0 K. Although temperature effects are not included, such corrections are expected to be small and should not change trends in the computed results (see: Bray, M. R.; Deeth, R. J. Paget, V. J. *Prog. React. Kinet.* **1996**, *21*, 169). Similarly entropy effects are not included. These should be most important for the formation of the NH_3 adducts; however changes in entropy contributions for the series of closely related reactions discussed here should be small, and it is anticipated that global trends should not be significantly affected by neglecting this term.
(45) (a) Lee, C.; Yang, W.; Parr, R. G. *Phys. Rev. B* **1988**, *37*, 785. (b) Johnson, B. G.; Gill, P. M. W.; Pople, J. A. *J. Chem. Phys.* **1993**, *98*, 5612. (c) Russo, T. V.; Martin, R. L.; Hay, P. J. *J. Chem. Phys.* **1994**, *101*, 7729.
(46) (a) Perdew, J. P.; Wang, Y. *Phys. Rev. B* **1986**, *33*, 8800. (b) Perdew, J. P.; Chevary, J. A.; Vosko, S. H.; Jackson, K. A.; Pederson, M. R.; Singh, D. J.; Fiolhais, C. *Phys. Rev. B* **1992**, *46*, 6671.

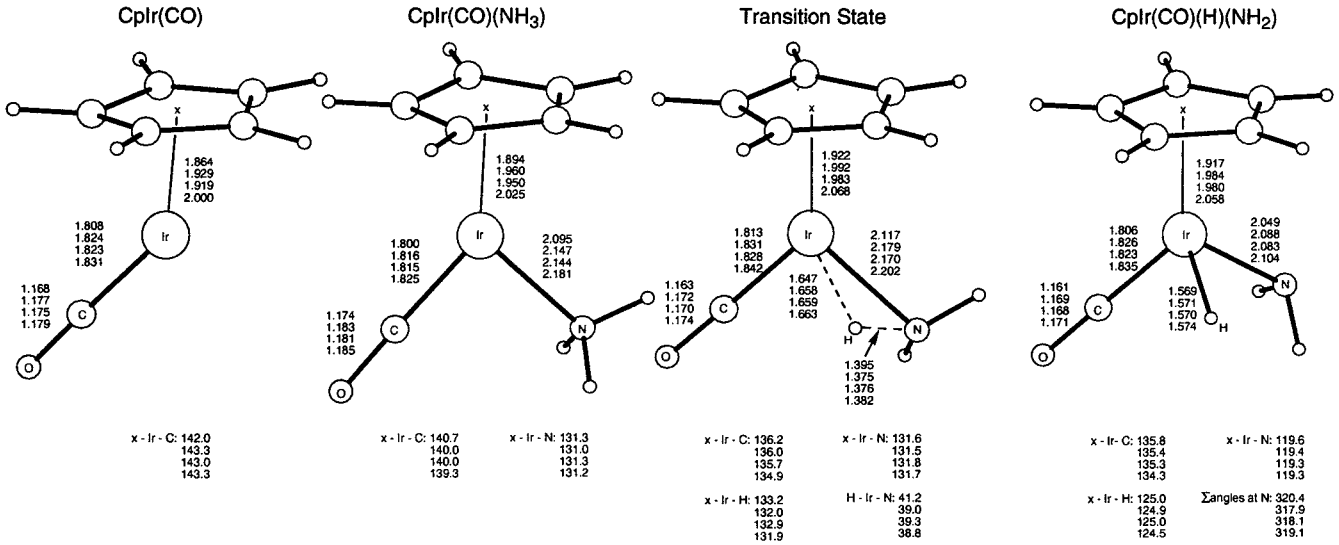

Figure 2. Optimized geometries (Å, deg) for stationary points located for the oxidative addition of NH_3 to CpIr(CO). Data correspond (from the top) to results computed with the LDA, BP, PW91, and BLYP functionals.

lengths when calculated with the LDA approach. Very similar geometries are calculated with the BP and PW91 functionals, while metal ligand distances are consistently longest with the BLYP functional. M−x (Cp centroid) and M−N bonds are generally shorter, but M−C(O) bonds are slightly longer for M = Ir. The major geometrical difference between the metals is computed in the transition states. For M = Ir the cleaving N−H bond is far shorter (∼1.38 Å compared to ∼1.53 Å for M = Rh) and the forming M−H bond is slightly longer, indicating an earlier transition state for the iridium system.

In general, geometries located with the BLYP functional are closest to the MP2 results of Musaev and Morokuma on CpRh(CO) + NH_3.[32c] However the product geometries in the present study exhibit a different orientation of the amido group (**1** vs **2**). Structure **1**, found here, may be preferred, as it improves push−pull

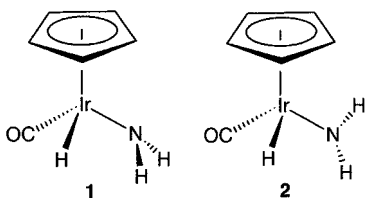

1 **2**

interactions between the amido and carbonyl ligands.[49,50] The amide nitrogen atoms in the products exhibit pyramidal geometries, the sum of angles around the nitrogen atom being 315.8° and 317.9° for M = Rh and Ir, respectively (BP calculations). This suggests no forward π-donation from the amide ligand exists, consistent with a saturated d^6 pseudo-octahedral product.[5a,11a]

Two different types of transition state structure for the oxidative addition of NH_3 to the unsaturated transition metal fragments in this study have been located at the BP level. These can be considered as arising from different motions of the NH_3 moiety during the oxidative addition process (see **3** and **4** below). In transition state

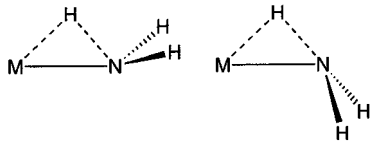

pyramidal planar

3 **4**

structure **3** the ammine ligand rotates as a whole and the {H···NH_2} moiety maintains an approximately pyramidal geometry at nitrogen. In transition state structure **4** the major movement involves the cleaving N−H bond and an approximately planar geometry for the {H···NH_2} group is found. These two structures can be viewed as being related by the inversion of the NH_3 group on the metal fragment and will be referred to as pyramidal and planar transition state geometries in the following. Apart from the different orientations of the NH_2 group, the geometries of these two types of transition state are very similar. For the reaction of CpM(CO) with NH_3 both types of transition states were found to connect to the ammine reactants and hydrido-amido products, with the planar transition states shown in Figure 1 found to be more stable by 1−2 kcal mol^{-1} (BP calculations).

Energy profiles for the reaction of CpRh(CO) + NH_3 computed with the four density functional approaches are compared in Figure 3a. The choice of functional appears most crucial in computing the relative binding energies of the NH_3 adduct, the trend being LDA ≫ PW91 ≈ BP > BLYP.[51] Thereafter the reaction profiles are very similar. Relative to the NH_3 adduct, activation energies range from 26.5 (LDA) to 29.4 kcal mol^{-1} (BLYP), while the energy change for the oxidative addition step is endothermic by around 16.5 kcal mol^{-1} for all functionals. With the exception of the LDA results, which are expected to overestimate metal−

(47) The magnitude of the HOMO−LUMO gaps (always > 1.5 eV) in the NH_3 adduct and subsequent transition states for NH_3 oxidative addition support the assertion that this process will occur preferentially on the singlet energy surface.

(48) Ziegler, T. *Chem. Rev.* **1991**, *91*, 651.

(49) Reoptimization of CpRhCO(H)(NH_2) with the NH_2 ligand rotated by 90° gave an energy 4.0 kcal mol^{-1} higher than the fully optimized structure (BP calculations). Upon removing the constraint in the NH_2 ligand orientation reoptimization produced the structure shown in Figure 1.

(50) Poulton, J. T.; Sigalas, M. P.; Folting, K.; Streib, W. E.; Eisenstein, O.; Caulton, K. G. *Inorg. Chem.* **1994**, *33*, 1476.

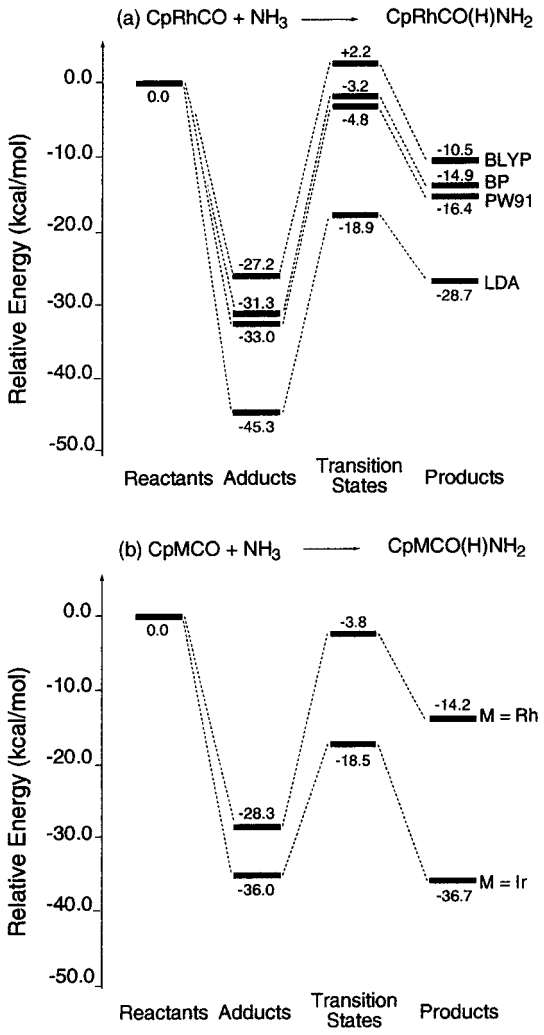

Figure 3. (a) Computed reaction profiles (kcal mol^{-1}) for the oxidative addition of NH_3 to CpRh(CO) calculated with the LDA, BP, PW91, and BLYP functionals. (b) Computed reaction profiles (kcal mol^{-1}) for the oxidative addition of NH_3 to CpM(CO) species (M = Rh, Ir) calculated with the BP functional. For comparison energies in (a) do not include a correction for zero-point energy, but this term is included in (b).

ligand bond strengths, the MP2 calculations of Musaev and Morokuma give a larger NH_3 binding energy (36.8 kcal mol^{-1}) and a higher activation energy relative to the ammine adduct (+41.9 kcal mol^{-1}). The oxidative addition step [$CpRh(CO)(NH_3) \rightarrow CpRh(CO)(H)(NH_2)$] is also more endothermic at the MP2 level (33.6 kcal mol^{-1}), part of which may arise from the different orientation of the amido group calculated here in the product. Relative energies calculated with the BLYP functional are closest to the MP2 results, although the overall oxidative addition process [$CpRh(CO) + NH_3 \rightarrow CpRh(CO)(H)(NH_2)$] is still more exothermic with the BLYP functional by 7 kcal mol^{-1}.

For the reaction of $CpIr(CO) + NH_3$ computed energy profiles vary with the density functional employed in a very similar way to that just described for the rhodium system. In Figure 3b therefore only the reaction profiles computed with the BP functional for the Rh and Ir systems are compared, while full details of the calculations performed with other functionals are available as Supporting Information. For M = Ir the NH_3 adduct is computed to be more strongly bound by 7.7 kcal mol^{-1}. In addition, the computed activation energy is lower by 7 kcal mol^{-1} and the oxidative addition step is computed to be slightly exothermic for the third-row metal complex. The thermodynamically more favorable reaction with iridium is consistent with the earlier transition state geometries noted above with that metal.

In summary, the choice of density functional to be employed is most crucial in calculating the NH_3 binding energy to the unsaturated CpM(CO) fragment. Thereafter, the oxidative addition step appears relatively insensitive to the functional used in terms of both the computed activation energy and the energy change associated with this process. CpIr(CO) binds NH_3 more strongly than does CpRh(CO), and the activation energy for N−H bond oxidative addition is also lower for M = Ir. Relative to the NH_3 adducts, the oxidative addition step is thermodynamically more favorable for M = Ir by 14.8 kcal mol^{-1}, although the overall process, relative to the isolated reactants, is exothermic for both metal fragments, with all functionals.

$M(PH_3)_2X + NH_3$ (M = Rh, Ir; X = H, Cl). A full study using all four density functional approaches was performed on the oxidative addition reaction of NH_3 to singlet $Ir(PH_3)_2Cl$. Computed trends in NH_3 binding energies with the four functionals were very similar to those described above for the CpM(CO) fragments. In addition, the energetics of the subsequent oxidative addition step were again found to be rather insensitive to the functional employed, and so only the results obtained with the BP functional will be discussed in the following. The full set of geometries and energies derived from the LDA, PW91, and BLYP calculations on the reaction of $Ir(PH_3)_2Cl$ with NH_3 are given as Supporting Information.

Computed geometries for the species involved in the oxidative addition of NH_3 to singlet $M(PH_3)_2Cl$ are given in Figure 4. The expected T-shaped geometry is computed for the d^8 $M(PH_3)_2Cl$ species, and a preference for a closed shell singlet electronic configuration is found for both metals (by 4.6 and 1.4 kcal mol^{-1} for M = Rh and Ir, respectively). For the reasons discussed above only the singlet state will be considered for reactivity. The computed geometries of these metal fragments, the NH_3 adducts, and the hydrido-amido species are similar for both metals, although some variation can be seen in the angles between equatorial ligands in the products. These product molecules are d^6 ML_5 species and as such would be expected to deviate from regular trigonal bipyramidal geometry.[52] With a single π-donor, X, d^6 ML_4X species exhibit a symmetrical C_{2v} Y shape, which facilitates π-donation into a vacant metal orbital.[53] The combination of two π-donor ligands in the present $M(PH_3)_2Cl(H)(NH_2)$ species produces a more distorted Y shape with effective C_s symmetry. The orientation of the amido ligand and the distortion toward a trigonal

(51) Although the NH_3 binding energy is far higher with the LDA functional, recalculation of the energies with the Becke and Perdew gradient corrections (i.e., an LDA+BP approach) gives very similar reaction energetics to those computed using the BP gradient corrections self-consistently.

(52) Riehl, J.-F.; Jean, Y.; Eisenstein, O.; Pélissier, M. *Organometallics* **1992**, *11*, 729.

(53) Macgregor, S. A.; MacQueen, D. *Inorg. Chem.* **1999**, *38*, 4868.

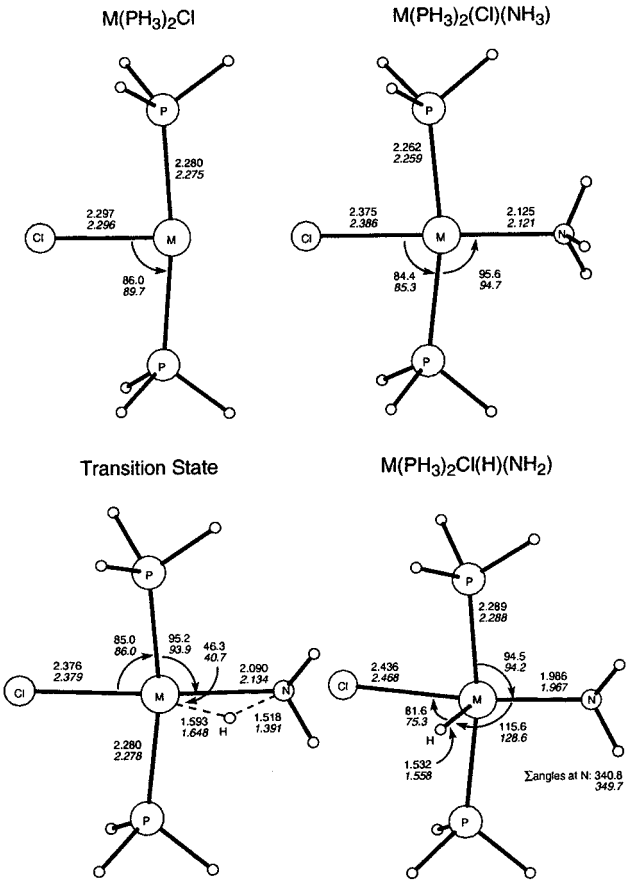

Figure 4. Optimized geometries (Å, deg) for stationary points located for the oxidative addition of NH_3 to $M(PH_3)_2Cl$ species (M = Rh, Ir) calculated with the BP functional. Values for M = Ir are given italics.

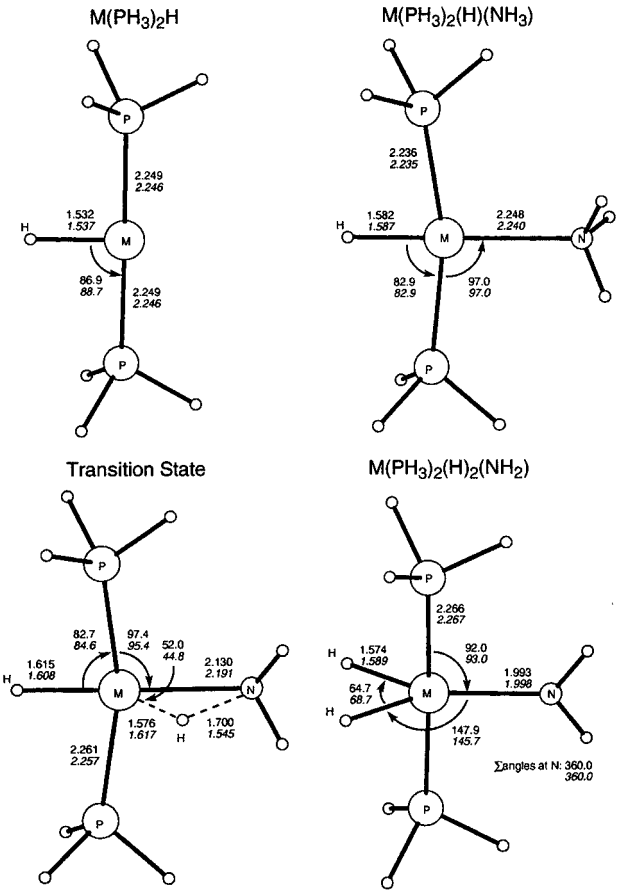

Figure 5. Optimized geometries (Å, deg) for stationary points located for the oxidative addition of NH_3 to $M(PH_3)_2H$ species (M = Rh, Ir) calculated with the BP functional. Values for M = Ir are given italics.

planar geometry at the nitrogen atom (the sum of angles at the nitrogen atom is 340.8° and 349.7° for M = Rh and Ir, respectively) are both indicative of some π-donation to the metal center.

Transition state calculations found a pyramidal structure to be favored over a planar alternative by 3.6 kcal mol^{-1} for M = Rh, while these two structures were of effectively the same energy for M = Ir. For both metals each type of transition state connects to the ammine reactants and hydrido-amido products. Pyramidal transition state structures are compared in Figure 4. As was found for the reaction of CpM(CO) with NH_3, computed transition state geometries were much earlier for the iridium system (N···H = 1.39 Å compared to 1.52 Å for M = Rh).

Optimized geometries for singlet $M(PH_3)_2H$ and subsequent stationary points along the NH_3 oxidative addition reaction profile are given in Figure 5. Calculated singlet−triplet energy gaps are 29.7 (Rh) and 32.9 kcal mol^{-1} (Ir). M−N bond lengths in the $M(PH_3)_2(H)(NH_3)$ adducts are about 0.12 Å longer compared to their chloro analogues, reflecting the higher *trans* influence of the hydride ligand. The hydrido-amido products exhibit effective C_{2v} symmetry with planar amido groups (the sum of angles at nitrogen being 360° for both metals). This is consistent with maximum π-donation from the amido group to the $IrH_2(PH_3)_2$ fragment and suggests the distorted shapes computed for the chloro analogues arise from π-competition effects. Despite this, M−N distances are about 0.02 Å longer in $Ir(PH_3)_2(H)_2(NH_2)$ compared to $Ir(PH_3)_2Cl(H)(NH_2)$. In this case only pyramidal transition state structures could be located at the BP level, as attempted optimization of planar structures collapsed to the pyramidal form. Transition state geometries are again earlier for M = Ir (N···H = 1.55 Å compared to 1.70 Å for M = Rh) although both N···H distances are much longer than those computed for X = Cl, with either metal.

Reaction profiles for the oxidative addition of NH_3 to $M(PH_3)_2X$ species are compared in Figure 6. For X = Cl, the NH_3 adduct is more strongly bound by 4.7 kcal mol^{-1} in the iridium complex. The subsequent oxidative addition step entails a lower activation energy (16.3 cf. 20.3 kcal mol^{-1}) and is slightly exothermic with the third-row metal complex (−1.4 kcal mol^{-1} compared to +13.4 kcal mol^{-1} for M = Rh). Similar differences between the metals are computed for the reaction with $M(PH_3)_2H$ species. Greater variation is found when the chloro and hydrido analogues of a given metal are compared. NH_3 adducts formed with $M(PH_3)_2H$ species are 13−16 kcal mol^{-1} less strongly bound than with $M(PH_3)_2Cl$, and while activation energies are only marginally higher for the $M(PH_3)_2H$ system, the oxidative addition step is thermodynamically more favorable when X = H. For M = Rh the oxidative addition step is endothermic by 9.1 kcal mol^{-1} but is exothermic by 6.0 kcal mol^{-1} for M = Ir.

$ML_2 + NH_3$ (M = Pd, Pt; L_2 = $(PH_3)_2$ or dpe). Geometries for the species involved in the oxidative

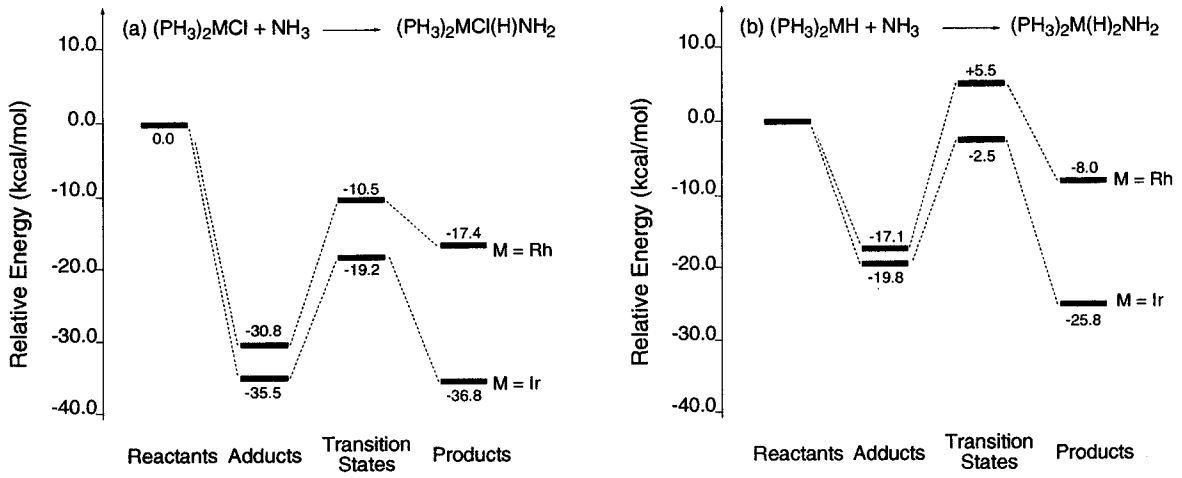

Figure 6. Computed reaction profiles (kcal mol^{-1}) for the oxidative addition of NH_3 to (a) $M(PH_3)_2Cl$ and (b) $M(PH_3)_2H$ species (M = Rh, Ir) calculated with the BP functional.

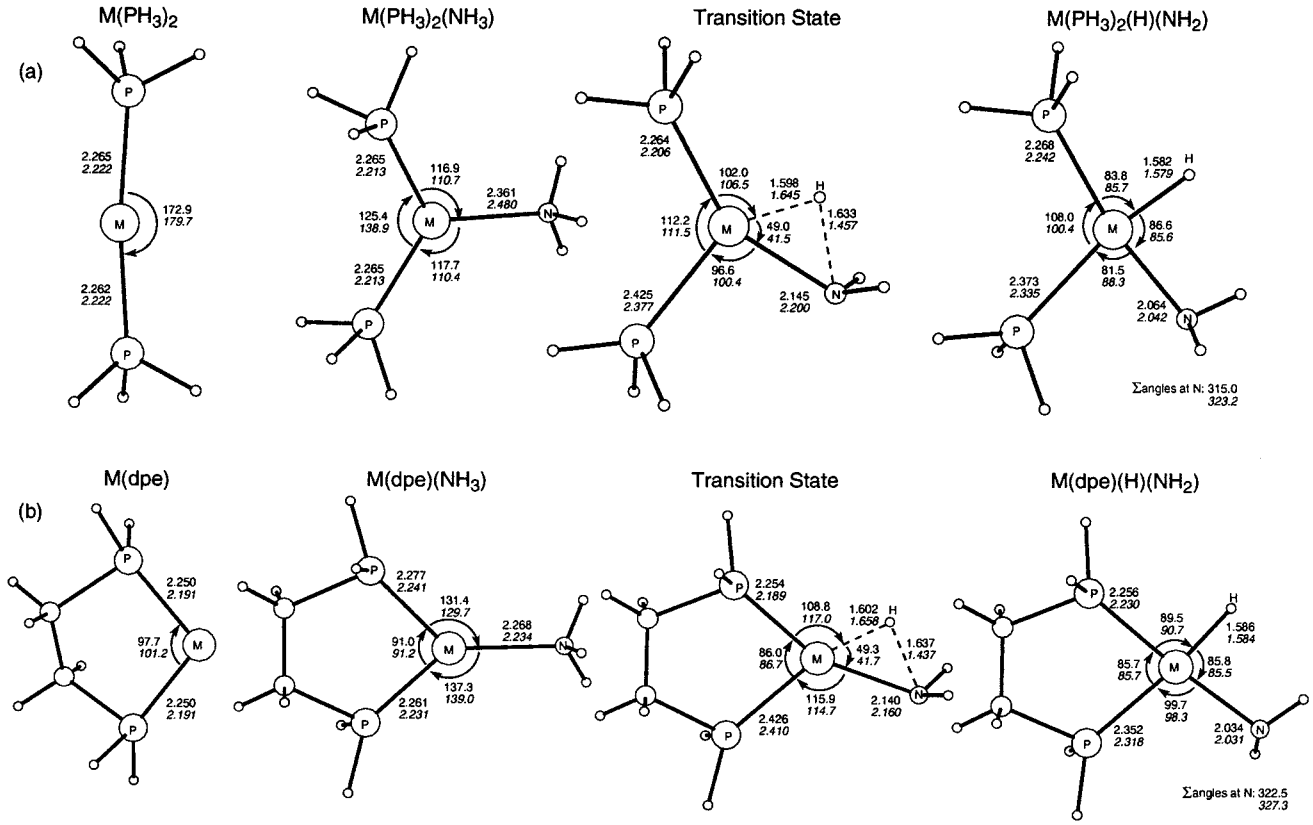

Figure 7. Optimized geometries (Å, deg) for stationary points located for the oxidative addition of NH_3 to (a) $M(PH_3)_2$ and (b) M(dpe) species (M = Pd, Pt) calculated with the BP functional. Values for M = Pt are given in italics.

addition of NH_3 to $M(PH_3)_2$ and M(dpe) species are given in Figures 7a and b, respectively. Only the more stable, singlet ML_2 fragments were considered.[34] $M(PH_3)_2(NH_3)$ adducts appear weakly bound with rather long M−N bonds, while much shorter M−N distances are computed in the M(dpe)(NH_3) species. All the computed hydrido-amido products exhibit a pyramidal amido group [sum of angles at nitrogen: with $M(PH_3)_2$, 315.0° (Pd) and 323.3° (Pt); M(dpe), 322.5° (Pd) and 327.3° (Pt)]. In these products M−P bonds *trans* to hydride are approximately 0.1 Å longer than those *trans* to amide. BP calculations indicate that pyramidal transition state structures are preferred over planar alternatives for both types of metal fragments (by about 4 kcal mol^{-1} when M = Pd but by less than 0.5 kcal mol^{-1} for M = Pt), and these are shown in Figure 7. The transition state structures are again earlier in the third-row metal systems [with $M(PH_3)_2$, N···H = 1.63 Å (Pd) and 1.46 Å (Pt); M(dpe), N···H = 1.64 Å (Pd) and 1.44 Å (Pt)].

Computed reaction profiles for the oxidative addition of NH_3 to the $M(PH_3)_2$ and M(dpe) fragments are compared in Figures 8a and b, respectively. Adducts formed between $M(PH_3)_2$ and NH_3 are weakly bound (M = Pd) or actually lie to slightly higher energy than the isolated reactants (M = Pt). Activation energies with $M(PH_3)_2$ species are very high, being 29.5 kcal mol^{-1} relative to the adduct for M = Pd and 23.8 kcal mol^{-1} for M = Pt. As found previously the overall oxidative addition process is thermodynamically more favorable for the third-row metal fragment, here by 14.7 kcal

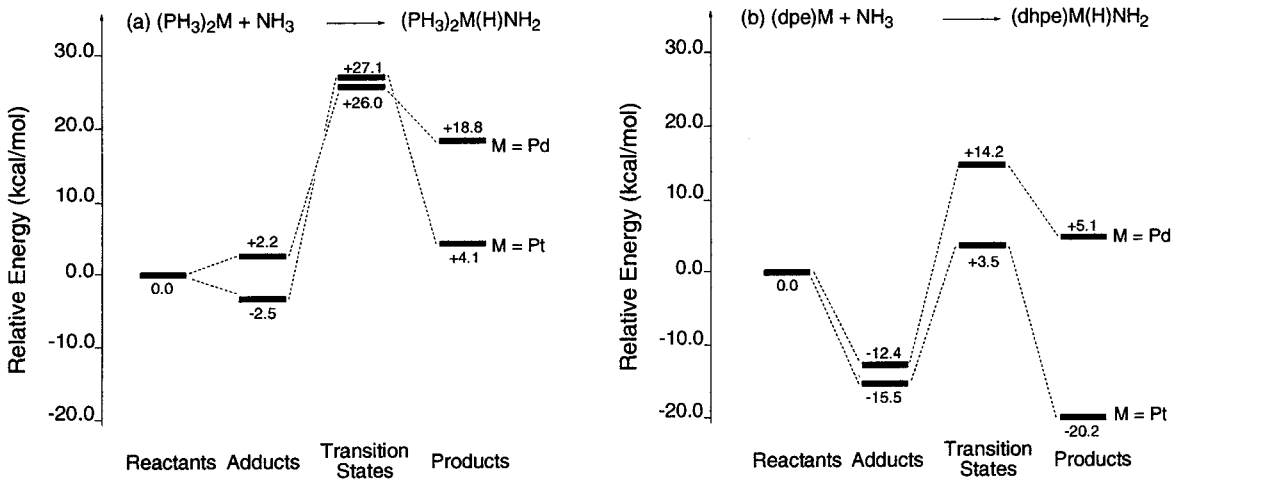

Figure 8. Computed reaction profiles (kcal mol^{-1}) for the oxidative addition of NH_3 to (a) $M(PH_3)_2$ and (b) M(dpe) species (M = Pd, Pt) calculated with the BP functional.

Table 1. Comparison of Crystallographically Determined and Computed (BP) Rh(III)− and Ir(III)−Amide Bond Distances (Å)

experimental		computed		
M = Rh	M−N	$CpM(CO)(H)(NH_2)$	$M(PH_3)_2Cl(H)(NH_2)$	$M(PH_3)_2(H)_2(NH_2)$
cis-$Rh(Cl)_2(o\text{-}Ph_2PC_6H_4NH_2)(o\text{-}Ph_2PC_6H_4NH)$[a]	2.018(5)	2.082	1.977	1.991
M = Ir				
$[Cp^*Ir(PMe_3)PhNH_2]_2 \cdot NaI(THF)$[b]	2.089(12), 2.106(11)	2.088	1.967	1.993
trans,cis-$[Ir(PPh_3)_2(H)_2(CO)(NC_4H_4)$[c]	2.154(4)			
$[(PEt_3)_2Ir(H)Cl(\mu\text{-}NH_2)]_2$[d]	2.10(1), 2.13(1)			
mer-$Ir(PMe_3)_3(H)Cl(NC_8H_6)$[e]	2.131(4)			

[a] Organ, G. J.; Cooper, M. K.; Henrick, K.; McPartlin, M. *J. Chem. Soc., Dalton Trans.* **1984**, 2377. [b] Reference 14. [c] Reference 23. [d] Reference 20. [e] Reference 15c, N *trans* to PMe_3.

mol^{-1}. In contrast to the previous cases, however, the overall oxidative addition process is calculated to be endothermic for both metals. Compared to $M(PH_3)_2$ species, the oxidative addition of NH_3 to M(dpe) fragments is much more favorable (Figure 8b), but especially so for M = Pt. NH_3 adduct formation is much stronger and activation energies for the oxidative addition step are also reduced (by 2.8 kcal mol^{-1} to 26.7 kcal mol^{-1} for M = Pd and by 4.8 kcal mol^{-1} to 19.0 kcal mol^{-1} for M = Pt). The oxidative addition step remains very endothermic for M = Pd (+17.5 kcal mol^{-1}) but becomes exothermic (−4.7 kcal mol^{-1}) for M = Pt.

Geometry optimizations after distortion along the unique imaginary mode of each transition state showed that both the pyramidal and planar structures connect to the expected hydrido-amido products. However distortion toward a reactant geometry gave varying results. Pyramidal transition states lead directly back to the ammine adduct for both $M(PH_3)_2$ and M(dpe). With $M(PH_3)_2$ the planar transition states lead to dissociation (i.e., $M(PH_3)_2 + NH_3$), while with the M(dpe) species new η^3-H,H,H adducts were located. These were computed to lie 7.1 (M = Pd) and 8.1 kcal mol^{-1} (M = Pt) above the conventional N-bound $M(dpe)NH_3$ adducts (see discussion).

Discussion

Geometries of Low-Valent Metal Ammine and Amido Complexes. The computed geometries reported here can be compared with those related structures that have been determined experimentally.[54] The BP computed Rh−N distances in $CpRh(CO)(NH_3)$ and $Rh(PH_3)_2Cl(NH_3)$ (2.154 and 2.125 Å, respectively) fall within the known range for neutral Rh(I) complexes featuring monodentate amine ligands. The computed Rh−N distance in $Rh(PH_3)_2H(NH_3)$ (2.248 Å) lies outside this range, presumably due to the high *trans* influence of the hydride ligand.[55] Only one complex of Ir(I) with a monodentate amine ligand has been crystallographically characterized: The Ir−N distance in $(dfepe)IrCl(NHEt_2)$ [dfepe = $(C_2F_5)_2PCH_2CH_2P(C_2F_5)_2$] is 2.185(8) Å,[56] somewhat longer than the computed values in $CpIr(CO)(NH_3)$ (2.147 Å) and $Ir(PH_3)_2Cl(NH_3)$ (2.121 Å) but shorter than that calculated for $Ir(PH_3)_2H(NH_3)$ (2.240 Å). A search of the Cambridge Structural Database revealed no entries for Pd(0)- or Pt(0)-amine complexes.

Known crystallographically characterized monodentate amide complexes for Ir(III), Pd(II), and Pt(II) metal centers are collated in Tables 1 and 2. In the Rh(III) example the amide is one arm of a chelating PN hybrid ligand, and this may explain the relatively large discrepancy with the computed Rh−N bond length in $CpRh(CO)(H)(NH_2)$. For $CpIr(CO)(H)(NH_2)$ the com-

(54) The United Kingdom Chemical Database Service: (a) Fletcher, D. A.; McMeeking, R. F.; Parkin, D. *J. Chem. Inf. Comput. Sci.* **1996**, *36*, 746. (b) Allen, F. H.; Kennard, O. *Chem. Des. Autom. News* **1993**, *8*, 31.

(55) The longest Rh(I)−N monodentate amine bond in the Cambridge Structural Database is 2.183(6) Å in $Rh(PPh_3)(CO)Cl(NHEt_2)$, where the amine is *trans* to the PPh_3 ligand: Petrucci, M. G. L.; Lebuis, A.-M.; Kakkar, A. K. *Organometallics* **1998**, *17*, 4966.

(56) Schnabel, R. C.; Roddick, D. M. *Inorg. Chem.* **1993**, *32*, 1513.

Table 2. Comparison of Crystallographically Determined and Computed (BP) Pd(II)− and Pt(II)−Amide Bond Distances (Å)

experimental		computed	
M = Pd		$M(PH_3)_2(H)NH_2$	$M(dpe)(H)(NH_2)$
$(tmeda)PdCl[N(SiMe_3)_2]$[a]	$Pd-N_{amide} = 2.043(6)$ $Pd-N_{trans\ Cl} = 2.102(7)$ $Pd-N_{trans\ N} = 2.104(7)$	$Pd-N_{amide} = 2.064$ $Pd-P_{trans\ H} = 2.373$ $Pd-P_{trans\ N} = 2.268$	$Pd-N_{amide} = 2.034$ $Pd-P_{trans\ H} = 2.352$ $Pd-P_{trans\ N} = 2.256$
trans-$Pd(PMe_3)_2(Ph)(NHPh)$[b]	$Pd-N = 2.116(13)$		
$(dppf)Pd(p\text{-}NMe_2C_6H_4)(NPh_2)$[c]	$Pd-N = 2.097(7)$ $Pd-P_{trans\ C} = 2.391(2)$ $Pd-P_{trans\ N} = 2.283(2)$		
M = Pt			
cis-$Pt(PEt_3)_2Cl(NPh_2)$[d]	$Pt-N = 2.09(2)$ $Pt-P_{trans\ Cl} = 2.277(4)$ $Pt-P_{trans\ N} = 2.2356)$	$Pt-N_{amide} = 2.042$ $Pt-P_{trans\ H} = 2.335$ $Pt-P_{trans\ N} = 2.242$	$Pt-N_{amide} = 2.031$ $Pt-P_{trans\ H} = 2.318$ $Pt-P_{trans\ N} = 2.230$
trans-$Pt(PEt_3)_2(H)(NHPh)$[e]	$Pt-N = 2.125(5)$		
$(dppe)Pt(CH_3)(NMePh)$[f]	$Pt-N = 2.097$ $Pt-P_{trans\ C} = 2.275$ $Pt-P_{trans\ N} = 2.209$		
cis-$Pt(PPh_3)_2[N(p\text{-}NO_2C_6H_4)_2]_2$[g]	$Pt-N = 2.033, 2.064$		

[a] Kim, Y.-J.; Choi, J.-C.; Osakada, K. J. *Organomet. Chem.* **1995**, *491*, 97. [b] Reference 10d. [c] Reference 10b. [d] Eadie, D. T.; Pidcock, A.; Stobart, S. R.; Brenna, E. T.; Cameron, T. S. *Inorg. Chim. Acta* **1982**, *65*, L111. [e] Reference 7a. [f] Reference 6d. Entry DAMBAO in the Cambridge Structural Database. [g] Li, W.; Barnes, C. L.; Sharp, P. R. *J. Chem. Soc., Chem. Commun.* **1990**, 1634. Entry KIBTIY in the Cambridge Structural Database.

Table 3. Energetics (kcal mol^{-1}) for the Oxidative Addition of NH_3 to Various Transition Metal Fragments Calculated with the BP Functional

	ΔE_{add}[a]	ΔE_{act}[b]	ΔE_{oxadd}[c]	ΔE_{total}[d]
$CpRh(CO) + NH_3$	−28.3	+24.5	+14.2	−14.2
$CpIr(CO) + NH_3$	−36.0	+17.5	−0.6	−36.7
$Rh(PH_3)_2Cl + NH_3$	−30.8	+20.3	+13.4	−17.4
$Ir(PH_3)_2Cl + NH_3$	−35.5	+16.3	−1.4	−36.8
$Rh(PH_3)_2H + NH_3$	−17.1	+22.6	+9.1	−8.0
$Ir(PH_3)_2H + NH_3$	−19.8	+17.3	−6.0	−25.8
$Pd(PH_3)_2 + NH_3$	−2.5	+29.5	+20.3	+18.8
$Pt(PH_3)_2 + NH_3$	+2.8	+23.8	+1.9	+4.1
$Pd(dpe) + NH_3$	−12.4	+26.7	+17.5	+5.1
$Pt(dpe) + NH_3$	−15.5	+19.0	−4.7	−20.2

[a] Calculated energy change for ammine adduct formation relative to free reactants. [b] Calculated activation energy for N−H bond cleavage relative to ammine adduct. [c] Calculated energy change for N−H bond cleavage step. [d] Calculated energy change for overall oxidative addition relative to free reactants.

puted Ir−N distance is in excellent agreement with the value derived from the related $[Cp^*Ir(PMe_3)PhNH_2]_2 \cdot NaI(THF)$ species. Computed M−N distances in the unsaturated $M(PH_3)_2X(H)(NH_2)$ species are shorter than any of the experimental structures which are all saturated species, providing further evidence for N→M π-donation in these model structures. The presence of arylamido or heterocyclic amido ligands in experimental structures results in trigonal planar geometries at the amido-N atom, and so these structures do not provide information about the extent of any N→M π-donation.[57] The computed M−N distances in the Pd(II) and Pt(II) *cis*-$M(PH_3)_2(H)(NH_2)$ and $M(dpe)(H)(NH_2)$ species fall either within or close to the range of metal−amide bond distances seen experimentally (Table 2). The relatively low *trans* influence of the NH_2 ligand indicated by the computed geometries (at least compared to hydride) is confirmed by the experimental structures which suggest the amide ligands have lower *trans* influences than chloride, methyl, and aryl ligands.

Energetics of Oxidative Addition. The results of the calculations presented here are summarized in Table 3 in terms of ΔE_{add} (the energy of ammine adduct formation), ΔE_{act} (the activation energy for NH_3 oxidative addition, computed relative to the ammine adduct), ΔE_{oxadd} (the energy change associated with the oxidative addition step), and ΔE_{total} (the overall energy change for the oxidative addition reaction, relative to the isolated reactants). ΔE_{total} is exothermic for CpM(CO) (M = Rh, Ir), $M(PH_3)_2X$ (M = Rh, Ir; X = H, Cl), and Pt(dpe), but is endothermic for $M(PH_3)_2$ (M = Pd, Pt) and Pd(dpe). Comparing second- and third-row analogues shows that ΔE_{total} is always more favorable for the third-row species. In addition, ΔE_{add} is higher for the third-row species (with the exception of the $M(PH_3)_2$ system), by between 2 and 8 kcal mol^{-1}, and ΔE_{oxadd} is more exothermic, by about 15 kcal mol^{-1} for the d^8 CpM(CO) and $M(PH_3)_2X$ systems, by 18.4 kcal mol^{-1} for $M(PH_3)_2$ and as much as 22.2 kcal mol^{-1} for M(dpe). ΔE_{act}, however, is lower with third-row metal species, the largest difference being 7.7 kcal mol^{-1} for M(dpe). The greater exothermicity of the oxidative addition step is reflected in the earlier transition states computed with the third-row species in which cleaving N···H bonds are between 0.12 and 0.2 Å shorter, and forming M···H bonds 0.04−0.07 Å longer, than in their second-row congeners.

The generally more favorable energetics for the NH_3 oxidative addition reaction computed with third-row metals are consistent with quantitative experimental data on related oxidative addition processes. An upper limit for the enthalpy change associated with the oxidative addition of cyclohexane to $Cp^*Ir(PMe_3)$ has been determined at −35.6 kcal mol^{-1},[58a] while that for the oxidative addition of a primary C−H bond of propane to $Cp^*Rh(PMe_3)$ is much smaller, at −18.6 kcal mol^{-1}.[58b] Similarly, lower limits for the enthalpies of oxidative addition of H_2 to $M(P^iPr_3)_2Cl$ are more exothermic for the iridium species (≤−48 compared to ≤−39 kcal mol^{-1} for the Rh analogue).[33e] No quantitative experimental data are available for N−H oxidative addition. However, the oxidative addition of NH_3 to low-valent transition metal centers has thus far only been achieved with iridium species,[20,21,24] while computation-

(57) In $(tmeda)PdCl[N(SiMe_3)_2]$ the sum of the angles at the amido nitrogen is 354.4°, while structures with bridging amido groups would not be expected to exhibit N−M π-donation.

ally the reactions of NH_3 with $Ir(PH_3)_2Cl$ and $CpIr(CO)$ are the most thermodynamically favorable of those studied here. The oxidative addition of NH_3 to Pt(0) complexes has been estimated to be approximately thermoneutral,[11b] in agreement with the calculations with the $Pt(PH_3)_2$ model, although the introduction of chelating ligands is computed to greatly promote this process. In addition, there is some experimental evidence to suggest that N−H bond oxidative addition is more facile for third-row metal centers. For example, oxidative addition of the amine moiety in $PPh_2(o\text{-}C_6H_4)$-NHR hybrid ligands was observed with Ir but not Rh.[19] N−H bond forming reductive elimination also occurs more readily for Pd- rather than Pt-hydrido-amides, consistent with the lower activation barriers computed for this process with *cis*-$Pd(PH_3)_2(H)(NH_2)$ and $Pd(dpe)(H)(NH_2)$ species compared to their Pt analogues.[7,59]

The computed results on NH_3 oxidative addition can also be placed in the context of other theoretical work on the oxidative addition reactions of other substrates to the transition metal complexes studied here.[32−35] When the reactivities of analogous second- and third-row transition metal complexes have been directly compared, these studies have consistently shown that the oxidative addition of a given substrate is more exothermic and proceeds with a smaller activation barrier with the third-row species.[35] These results have been rationalized in terms of the atomic configurations of the metal atoms involved. For example, in group 10 ML_2 species promotion of an electron from the formally d^{10} configuration to a d^9s^1 state is required before the two new bonds resultant upon oxidative addition can be formed. The relative energies of the molecular d^{10} and d^9s^1 states reflect those configurations in the free atoms, and as Pd has a d^{10} ground state and a relatively high lying d^9s^1 excited state, but Pt has a d^9s^1 ground state, the oxidative addition reaction is much more favorable for PtL_2 species.[34b−d] Similarly, the greater efficiency of alkane activation by CpIr(CO) compared to CpRh(CO) can be understood in terms of the greater accessibility of the triplet state in the former.[32d]

To compare the abilities of different unsaturated transition metal fragments to effect the oxidative addition of NH_3, a further rationale of oxidative addition processes in terms of the nature of the frontier molecular orbitals of the metal species involved will be presented.[60] The oxidative addition of CH_4 to a generic ML_n fragment of C_{2v} symmetry will be used to illustrate this approach. During the oxidative addition process the metal center must act as both a Lewis acid and a Lewis base. The early stages of the reaction are characterized by donation of electron density from the occupied C−H σ-bonding orbital to a suitable acceptor orbital on the metal ($2a_1$, see Scheme 1). This may be offset by 4e destabilizing interactions between the C−H σ-bonding orbital and occupied metal-based orbitals of local σ-symmetry ($1a_1$), and the balance of these interactions will determine the strength of any alkane precursor complex that forms. For oxidative addition to proceed, sufficient π-back-donation into a C−H antibonding σ^* orbital must occur, and this may require both a reorientation of CH_4 and a deformation of the ML_n fragment, motions that may incur a significant activation energy. An ideal unsaturated metal fragment for oxidative addition will therefore have a high lying occupied orbital analogous to the b_2 orbital of Scheme 1 (i.e., be a good Lewis π-base), a low lying acceptor orbital analogous to the $2a_1$ orbital (a good Lewis acid), and preferably occupied a_1 orbitals which minimize destabilizing interactions with the C−H σ-bonding orbital.

Scheme 1

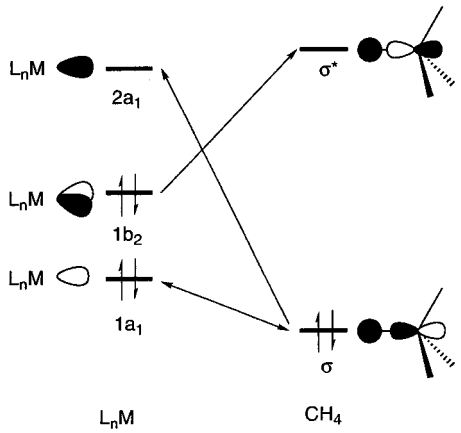

Using this model, the role of the metal fragment in promoting oxidative addition processes can be understood. Thus, Ziegler and co-workers have shown that CpML fragments (M = Rh, Ir: L = CO, PH_3) are ideally set up for oxidative addition, not only through the presence of a low-lying a_1-type acceptor orbital and high-lying b_2-type donor orbital (good Lewis acidity and basicity, respectively) but also through an absence of high lying occupied a_1-type orbitals that can interact effectively with the substrate.[32a] $M(PH_3)_2X$ species, where X is a π-donor, have been shown to have reduced activation barriers and more exothermic reactions compared to when X is a strong σ-donor such as H or CH_3.[33c,f] The weaker *trans*-influence π-donor not only makes the metal fragment a better Lewis acid, but also increases Lewis basicity by destabilizing the occupied b_2-type donor orbital. Finally, the use of chelating ligands in group 10 ML_2 species greatly facilitates oxidative addition by imposing a bent, pseudo-C_{2v} geometry on the metal center. This causes a stabilization of an a_1 acceptor orbital and a destabilization of an occupied b_2 metal-based donor orbital, improving both the Lewis acidity and basicity of the metal center compared to those in linear monodentate analogues.[34g]

(58) (a) Stoutland, P. O.; Bergman, R. G.; Nolan, S. P.; Hoff, C. D. *Polyhedron* **1988**, *7*, 1429. (b) Jones, W. D.; Feher, F. J. *Acc. Chem. Res.* **1989**, *22*, 91. Both figures are based on activation energies for the reverse reductive elimination process. For $Cp^*(PMe_3)Ir(H)(c\text{-}C_6H_{11})$ the figure of −35.6 kcal mol^{-1} is derived from the activation *enthalpy* for reductive elimination. The true enthalpy change for oxidative addition will be reduced by the strength of the alkane precursor that is formed, estimated to be between 2 and 5 kcal mol^{-1}. See ref 63. For $Cp^*(PMe_3)Rh(H)(n\text{-}C_3H_7)$ a value of −18.6 kcal mol^{-1} arises from the *free energy* of activation for reductive elimination. The enthalpy change for oxidative addition will be affected by both the strength of any alkane presursor complex and the unfavorable entropy of this process, effects that should to some extent counteract each other.

(59) Note however that amine reductive elimination from *trans*-$M(PR_3)(H)NHAr$ species only occurs readily upon addition of 2e donor ligands for both M = Pd and Pt and therefore presumably involves five-coordinate intermediates. However, insertion of $H_2C{=}CHCN$ into the M−N bond was observed for the Pt species, suggesting this process to be more competitive with N−H bond reductive elimination for that metal compared to the Pd analogue.

(60) (a) Saillard, J.-Y.; Hoffmann, R. *J. Am. Chem. Soc.* **1984**, *106*, 2006. (b) Macgregor, S. A.; Eisenstein, O.; Whittlesey, M. K.; Perutz, R. N. *J. Chem. Soc., Dalton Trans.* **1998**, 291.

Consistent with this previous work the NH_3 oxidative addition reaction profiles computed here show both reduced activation energies and higher reaction exothermicities with third-row transition metal fragments. Comparing the $M(PH_3)_2H$ and $M(PH_3)_2Cl$ species shows the introduction of a π-donor also results in small reductions in ΔE_{act}. However, in contrast to previous work on alkanes, the energy of the oxidative addition step (ΔE_{oxadd}) is more endothermic with $M(PH_3)_2Cl$ species. In addition, although for ML_2 species the use of a chelating phosphine dramatically increases exothermicity compared to the $M(PH_3)_2$ models, reductions in activation energies are relatively modest compared to the computed effect this change has on alkane activation.[61] More generally, it is interesting to note that for all four of the most reactive third-row fragments—CpIr(CO), the $Ir(PH_3)_2X$ species, and Pt(dpe)—relatively little variation in ΔE_{act} is seen, with computed values in the range 16−19 kcal mol^{-1}. This point, as well as the more favorable thermodynamics of NH_3 oxidative addition calculated with third-row complexes, will be discussed below.

Metal−Amide and −Hydride Bond Strengths. The computational results provide the opportunity to quantify the greater thermodynamic preference for NH_3 oxidative addition exhibited by third-row transition metal fragments in terms of the homolytic bond dissociation energies of the metal−amide (D_{M-NH_2}) and metal−hydride (D_{M-H}) bonds that are formed in this process. These can be estimated using the approach previously described by Koga and Morokuma[62] from the energy change for the NH_3 oxidative addition reaction, ΔE_1:

$$L_nM + NH_3 \rightarrow L_nM(H)(NH_2) \cdots \Delta E_1$$

$$\Delta E_1 = -D_{M-NH_2} - D_{M-H} + D_{H-NH_2}$$

where a computed value for D_{M-H} can be estimated from the energy change of the analogous H_2 oxidative addition reaction, ΔE_2:

$$L_nM + H_2 \rightarrow L_nM(H)_2 \cdots \Delta E_2$$

$$\Delta E_2 = -2D_{M-H} + D_{H-H}$$

D_{H-NH_2} and D_{H-H} are computed directly with the BP functional to be 104.9 and 105.1 kcal mol^{-1}, respectively, and compare with experimental values of 107.4 and 104.2 kcal mol^{-1}.

Computed values of D_{M-NH_2} and D_{M-H} for CpM(CO)(H)(NH_2), $M(PH_3)_2X(H)(NH_2)$ (M = Rh, Ir; X = H, Cl), and *cis*-$M(PH_3)_2(H)(NH_2)$ and M(dpe)(H)(NH_2) (M = Pd, Pt) species are summarized in Table 4, along with the corresponding values of ΔE_1 and ΔE_2. The value of D_{Pt-H} derived from $(PH_3)_2Pt(H)_2$ is in good agreement with that computed by Sakaki et al. at the MP4SDQ//MP2 level (58.8 kcal mol^{-1} [34h]), while values of D_{Rh-NH_2} and D_{Rh-H} in CpRh(CO)(H)(NH_2) are slightly higher than those reported previously by Morokuma and Musaev in their study.[32c] The computed data show that the more favorable thermodynamics calculated for the oxidative addition of NH_3 to third-row transition metal complexes arises via contributions from both stronger M−NH_2 and M−H bonds. For group 9 systems M−NH_2 bonds are between 9 and 13 kcal mol^{-1} stronger in the Ir species, while the Pt−NH_2 bonds in *cis*-$Pt(PH_3)_2(H)(NH_2)$ and Pt(dpe)(H)(NH_2) are respectively 6.1 and 11.6 kcal mol^{-1} stronger than in the Pd analogues. Within the group 9 species trends in Rh− and Ir−NH_2 bond strengths track the degree of N→M π-donation suggested by the geometry of the amide ligand. Thus CpCO(H)M−NH_2 bonds are weakest (pyramidal-N, no π-donation), $(PH_3)_2(H)_2M-NH_2$ bonds are strongest (planar N, full π-donation), and $(PH_3)_2Cl(H)M-NH_2$ bond strengths lie between these extremes (distorted-planar N due to π-competition effects, intermediate π-donation). Trends between second- and third-row analogues for D_{M-H} are similar to those for D_{M-NH_2}, although the relative strengthening of the third-row M−H bonds is slightly greater. Computed Rh−H and Ir−H bond strengths are in reasonable agreement with experimental values derived from related complexes. Lower limits for the average M−H bond strength in $M(P^iPr_3)_2(H)_2Cl$ complexes are ≥72 (Rh) and 76 kcal mol^{-1} (Ir).[33e] The Ir−H bond in Cp*(PMe$_3$)Ir(H)(R) species has a bond dissociation energy of 74 kcal mol^{-1} (R = *c*-C_6H_{11} [58a]) and 72.9 ± 4.3 kcal mol^{-1} (R = H[63]). Ir−H homolytic bond strengths have also been determined for a series of $[CpIrL_2H]^+$ complexes (L = CO, PR_3) to lie in the range 70−75 kcal mol^{-1}.[64] The only Pt−H bond dissociation energy determined experimentally is for *trans*-$Pt(PPh_3)_2Cl(H)$ and is 73.4 ± 8.8 kcal mol^{-1}.[65] This is somewhat higher than the computed D_{Pt-H} values, possibly due to the lower *trans* influence of Cl compared to the PH_3 ligand used in the calculations.

For the group 9 species trends in D_{M-H} complement those in D_{M-NH_2}, weakening as the latter increases. In the CpM(CO)(H)(NH_2) complexes D_{M-H} is computed to be about 25 kcal mol^{-1} stronger than D_{M-NH_2}. This difference is reduced to 21 kcal mol^{-1} for $M(PH_3)_2Cl(H)(NH_2)$ species and to only 8 kcal mol^{-1} for $Rh(PH_3)_2(H)_2(NH_2)$, while parity is almost achieved in $Ir(PH_3)_2(H)_2(NH_2)$. For the group 10 species D_{M-H} is calculated

Table 4. Values (kcal mol^{-1}) for ΔE_1, ΔE_2, D_{M-NH_2}, and D_{M-H} Calculated with the BP Functional

	ΔE_1	ΔE_2	D_{M-H}	D_{M-NH_2}
CpRh(CO)(H)(NH_2)	−14.2	−38.3	71.7	47.4
CpIr(CO)(H)(NH_2)	−36.6	−63.8	84.0	57.5
$Rh(PH_3)_2Cl(H)(NH_2)$	−17.4	−38.5[a]	71.8	50.5
$Ir(PH_3)_2Cl(H)(NH_2)$	−36.8	−58.2[a]	81.6	60.1
$Rh(PH_3)_2(H)_2(NH_2)$	−8.0	−15.8[b]	60.4	52.5
$Ir(PH_3)_2(H)_2(NH_2)$	−25.8	−26.4	65.7	65.0
cis-$Pd(PH_3)_2(H)(NH_2)$	+18.8	+3.0	51.0	35.1
cis-$Pt(PH_3)_2(H)(NH_2)$	+4.1	−14.1	59.6	41.2
Pd(dpe)(H)(NH_2)	+5.1	−9.4	57.3	42.5
Pt(dpe)(H)(NH_2)	−20.2	−36.8	71.0	54.1

[a] $(PH_3)_2M(H_2)Cl$ most stable with a Y_{Cl} shape and therefore not isostructural with $(PH_3)_2M(H)_2(NH_2)$. [b] $(PH_3)_2Rh(H)_3$ is computed to be a dihydrogen complex with the BP functional.

(61) For example, for the oxidative addition of CH_4 the introduction of a model chelating phosphine has been calculated at the MP4SDQ level to increase reaction exothermicities by more than 30 kcal mol^{-1} for both PdL_2 and PtL_2 systems and to reduce activation barriers by more than 14 kcal mol^{-1} (Pd) and by more than 23 kcal mol^{-1} (Pt). See ref 34g.

(62) Koga, N.; Morokuma, K. *J. Am. Chem. Soc.* **1993**, *115*, 6883.

(63) Nolan, S. P.; Hoff, C. D.; Stoutland, P. O.; Newman, L. J.; Buchanan, J. M.; Bergman, R. G.; Yang, G. K.; Peters, K. S. *J. Am. Chem. Soc.* **1987**, *109*, 3143.

(64) Wang, D.; Angelici, R. J. *J. Am. Chem. Soc.* **1996**, *118*, 935.

(65) Mortimer, C. T. *Rev. Inorg. Chem.* **1984**, *6*, 233.

to be between 15 and 17 kcal mol^{-1} stronger in the third-row complexes. Single homolytic bond strengths between late transition metals and anionic ligands (D_{M-X}) have often been discussed in terms of a 1:1 correlation between D_{M-X} and D_{H-X}, first highlighted by Bryndza and Bercaw and co-workers.[66] As D_{H-H} and D_{H-NH_2} are similar, strict application of this theory would predict comparable values for D_{M-H} and D_{M-NH_2} in CpM(CO)(H)(NH_2) and the group 10 ML_2(H)(NH_2) species (i.e., complexes where no N→M π-bonding is evident). The large differences in D_{M-H} and D_{M-NH_2} computed for these species could arise from several sources. First, M−H bonds were found in the original Bryndza/Bercaw analysis to be anomalously strong, possibly due to the absence of any electrostatic component in the parent HX species (i.e., H_2).[67] Second, filled−filled interactions may weaken M−X bonds. This effect has been suggested to contribute to the weakening of M−CH_3 bonds relative to M−H bonds in complexes where M is a middle to late transition metal.[68] This factor would be expected to be even more significant for amide ligands bearing a lone pair. Recently however, Bergman, Andersen, and co-workers have emphasized the role of electronegativities in producing stronger Ni−O bonds compared to Ni−N bonds in a series of isosteric Ni-aryl-oxides and -amides.[69] From the present study it is apparent that forward N→M π-donation is responsible for stronger M−amide bonds in the formally unsaturated M(PH_3)$_2$X(H)(NH_2) systems, but the extent to which filled−filled interactions serve to weaken these bonds in saturated species is not clear.

Activation Energies for NH_3 Oxidation Addition. Musaev and Morokuma in their study of the oxidative addition of NH_3 to CpRh(CO) have suggested that the stability of the precursor CpRh(CO)(NH_3) adduct results in a prohibitively high activation energy (+42 kcal mol^{-1}) for the oxidative addition process and therefore that the hydrido-amido products will be kinetically inaccessible.[32c] The lowest activation barrier computed here is +16.3 kcal mol^{-1} for the Ir(PH_3)$_2$Cl fragment. As experimental analogues of this species are capable of NH_3 oxidative addition, the fact that similar activation energies are computed for other model metal fragments [CpIr(CO), Ir(PH_3)$_2$H, and Pt(dpe)] suggests these species may also be able to effect this reaction. Schultz and Milstein have suggested that activation barriers may be linked to the ease of "slippage" of the bound NH_3 ligand to an η^2-NH form.[21c] In their study, NH_3 oxidative addition was observed for Ir(PEt_3)$_2$Cl, where the PEt_3 ligands are expected to be *cis*, but not with Ir(P^iPr_3)$_2$Cl, where steric effects force a *trans* configuration. The greater Lewis acidity of the latter species, in which chloride is *trans* to the ammine binding site, was thought to make reorientation of the NH_3 ligand a high-energy process and an alternative C−H bond activation reaction with ethene was observed in this case. However, the computed results presented here for the M(PH_3)$_2$X species suggest that the nature of the ligand *trans* to the ammine binding site has relatively little influence on the computed activation energy for NH_3 oxidative addition. Thus, compared to Ir(PH_3)$_2$Cl, Ir(PH_3)$_2$H produces the expected lower value of ΔE_{add}, but ΔE_{act} remains higher by 1 kcal mol^{-1}. ΔE_{oxadd} on the other hand is more favorable with Ir(PH_3)$_2$H by 4.7 kcal mol^{-1}, a result that can be explained through a combination of ammine adduct destabilization and stabilization of the Ir(PH_3)$_2$(H)(NH_2) products (relative to the Ir(PH_3)$_2$(H)(NH_3) adduct) through enhanced π-donation from the amide.

More generally, no correlation between the strength of ammine adduct formation and the subsequent activation energy can be seen in the computed results. Thus, although adduct formation is generally stronger with third-row fragments, activation energies are lower. Focusing on the more reactive third-row fragments shows that strong Lewis acids (CpIr(CO) or Ir(PH_3)$_2$Cl) require activation energies similar to those computed for much less Lewis acidic metal fragments [Ir(PH_3)$_2$H and Pt(dpe)]. ΔE_{add} varies by over 20 kcal mol^{-1} with these species, but ΔE_{act} falls within a relatively narrow range (+16.3 to +19.0 kcal mol^{-1}).

To account for this lack of correlation between ΔE_{add} and ΔE_{act}, the overall NH_3 oxidative addition reaction will be considered as a two-stage process. Initially reorientation of the ammine ligand must occur before the second stage—N−H bond activation—can proceed to give the oxidative addition product. The effect of the metal fragment on both these processes must be taken into account. Reorientation of the ammine ligand, either through NH_3 rotation or inversion at the N atom, will entail loss of the σ-bonding interaction between the nitrogen lone pair and the metal center. This process would be expected to be disfavored by strongly Lewis acidic metal fragments such as CpIr(CO) and Ir(PH_3)$_2$Cl, but to become relatively more facile with poorer Lewis acids such as Pt(dpe) or Ir(PH_3)$_2$H. Once the NH_3 moiety is correctly oriented for N−H bond activation, however, the general factors that promote oxidative addition reactions described previously will become important. For CpIr(CO) and Ir(PH_3)$_2$Cl the N−H bond activation process should therefore be relatively easy. Compared to Ir(PH_3)$_2$Cl, N−H bond activation by Ir(PH_3)$_2$H will be less favored due to the poorer π-basicity of the latter. Overall the variation in the energetics of the two stages of the NH_3 oxidative addition process appear to cancel each other out, producing similar activation energies for these two Ir(PH_3)$_2$X species. Similarly, compared to species such as CpIr(CO), the lower Lewis acidity of Pt(dpe) would disfavor the N−H bond activation step, with similar activation energies again being computed with these two very different fragments.

In an attempt to quantify these ideas, energy profiles for the reorientation of the NH_3 ligand in the Ir(PH_3)$_2$Cl(NH_3) and Pt(dpe)(NH_3) complexes have been computed. The motion studied corresponds to rotation of the NH_3 ligand about an axis passing through the N atom perpendicular to the original M−N bond in the NH_3 adducts. Rotation profiles were built up by systematic

(66) Bryndza, H. E.; Fong, L. K.; Paciello, R. A.; Tam, W.; Bercaw, J. E. *J. Am. Chem. Soc.* **1987**, *109*, 1444.
(67) Labinger, J. A.; Bercaw, J. E. *Organometallics* **1988**, *7*, 926.
(68) Ziegler, T.; Cheng, W.; Baerends, E. J.; Ravenek, W. *Inorg. Chem.* **1988**, *27*, 3458.
(69) Holland, P. L.; Andersen, R. A.; Bergman, R. G.; Huang, J.; Nolan, S. P. *J. Am. Chem. Soc.* **1997**, *119*, 12800.
(70) Both TS2 and TS3 were computed to be slightly less stable than the η^1-H and η^3-H,H,H adducts, respectively, before the inclusion of zero-point energies, but become relatively slightly more stable when this correction is included. Computed energies both with and without this correction are therefore given in Figure 10.

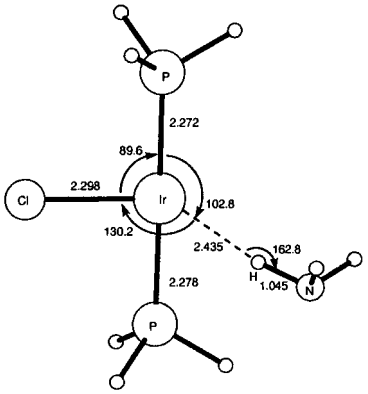

Figure 9. Optimized geometry (Å, deg) for the η^1-H transition state for NH_3 rotation for $Ir(PH_3)_2Cl(NH_3)$ calculated with the BP functional.

variation of one M−N−H angle. This study also aimed to locate any alternative NH_3 adducts that might be formed where the NH_3 moiety could bind to the metal fragment through donation of N−H bonding electrons to the metal center. Such species would be analogous to methane σ-complexes and could be akin to Milstein's postulated "slipped η^2-NH" species. Note that for Pt(dpe)(NH_3) an η^3-H,H,H adduct has already been located from the characterization of the planar transition state for NH_3 oxidative addition.

For the $Ir(PH_3)_2Cl(NH_3)$ system a single stationary point was located which corresponded to a transition state for the NH_3 rotation process (Figure 9). This species has an η^1-H form and is computed to lie 32.2 kcal mol^{-1} above the conventional $Ir(PH_3)_2Cl(NH_3)$ adduct. In addition, this structure lies about 16 kcal mol^{-1} above the near equienergetic alternative transition states (pyramidal and planar) for NH_3 oxidative addition and cannot therefore be involved in that process. As no other alternative NH_3 adducts were located, the oxidative addition of NH_3 to $Ir(PH_3)_2Cl$ appears to involve a concerted NH_3 reorientation/N−H bond activation sequence.

For the Pt(dpe)(NH_3) system several stationary points along the NH_3 rotation profile were located, and geometries and relative energies are given in Figure 10. A minimum corresponding to an η^1-H adduct was computed in which the Pt−H−N angle is almost linear (173.4°). This species lies 12.0 kcal mol^{-1} above the conventional Pt(dpe)(NH_3) adduct and connects directly to this species via TS1 ($E = +12.4$) A second transition state structure, TS2 ($E = +11.6$ kcal mol^{-1} [70]), connects to an η^3-H,H,H adduct ($E = +8.1$ kcal mol^{-1}), from which a third transition state (TS3, $E = +7.9$ kcal mol^{-1}) corresponding to nitrogen atom inversion must be cleared to complete the NH_3 rotation process.

The η^3-H,H,H adduct is the same species as that located previously from the planar transition state for NH_3 oxidative addition, and therefore this species corresponds to an intermediate for this process, which proceeds via stepwise NH_3 inversion followed by N−H

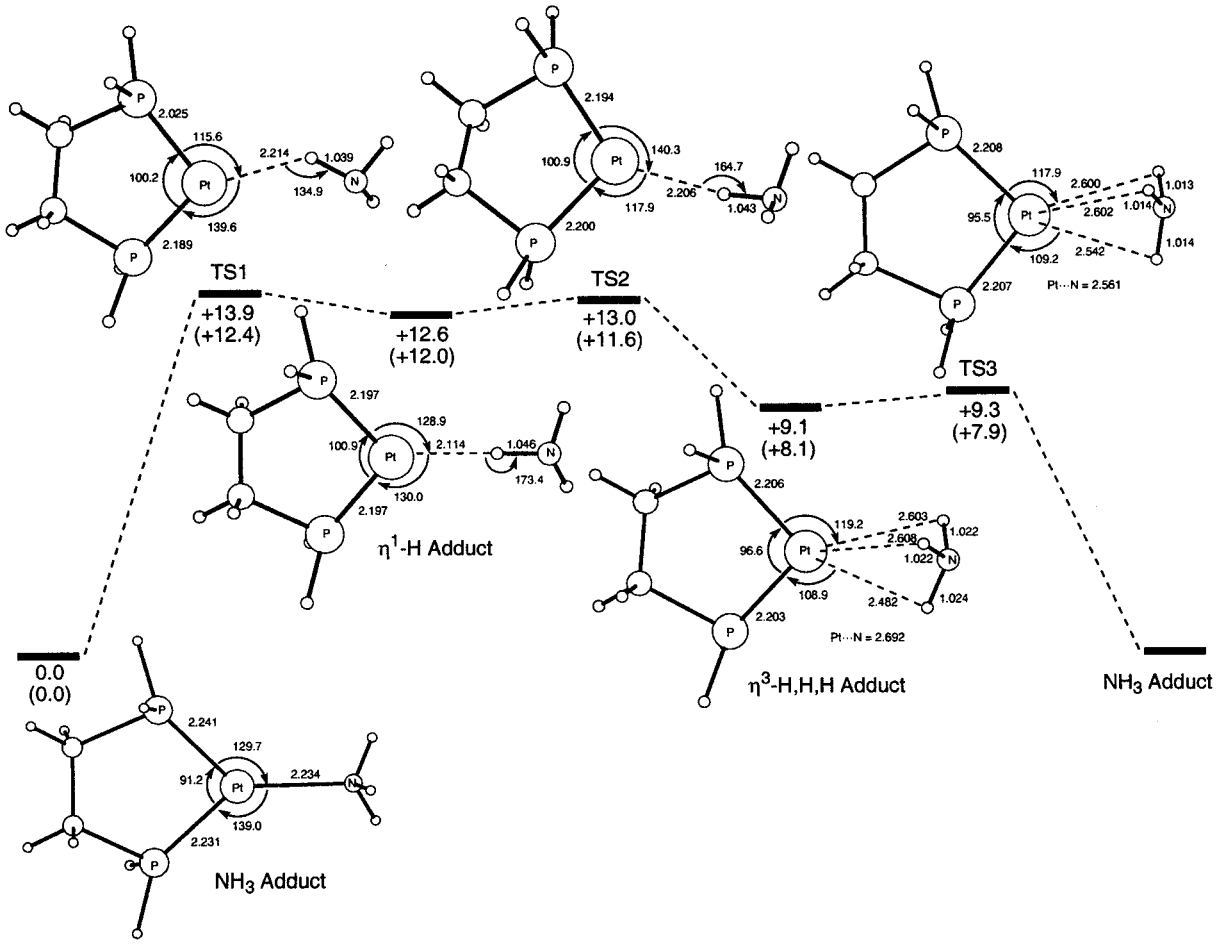

Figure 10. Optimized geometries (Å, deg) and relative energies (kcal mol^{-1}) for stationary points along the NH_3 rotation profile for Pt(dpe)(NH_3) calculated with the BP functional. Energies are relative to the N-bound Pt(dpe)(NH_3) adduct set to zero and include a correction for zero-point energies in parentheses.

bond activation. The role of the η^1-H adduct in NH_3 oxidative addition is less clear. The near linear Pt···H−N geometry in this species is quite unlike that found in the pyramidal transition state for NH_3 oxidative addition (where the corresponding Pt···H−N angle is 82.7°), and characterization of that transition state geometry via distortion along its unique imaginary mode and subsequent geometry optimization lead directly to the conventional Pt(dpe)(NH_3) adduct and Pt(dpe)(H)(NH_2) product. Therefore, despite lying 7 kcal mol^{-1} below the transition states for NH_3 oxidative addition, there is no evidence for the direct intermediacy of the η^1-NH species in this process. A concerted NH_3 reorientation/N−H bond activation process is therefore likely for the NH_3 oxidative addition reaction with Pt(dpe)(NH_3) when a pyramidal transition state structure is involved.

The species located along these NH_3 rotation profiles for Ir(PH_3)$_2$Cl(NH_3) and Pt(dpe)(NH_3) give an indication of the relative ease of NH_3 reorientation in the NH_3 oxidative addition process. Pt(dpe)(NH_3) reorientation to an η^3-H,H,H adduct requires an activation energy of 8 kcal mol^{-1}, and the subsequent N−H bond activation (via a planar transition state) incurs a further barrier of 11 kcal mol^{-1}. The η^1-H species are probably not directly involved in the oxidative addition process but indicate that full NH_3 rotation in Ir(PH_3)$_2$Cl(NH_3) requires an activation energy of 32.2 kcal mol^{-1}, while for Pt(dpe)(NH_3) the figure is around 12 kcal mol^{-1}. These results are consistent with the idea that for Ir(PH_3)$_2$Cl, and similar strongly Lewis acidic metal fragments, the activation energy for NH_3 oxidative addition corresponds mostly to the energy required for NH_3 reorientation. For Pt(dpe) and weaker Lewis acidic metal fragments NH_3 reorientation is relatively more facile, but the subsequent N−H bond activation requires a further contribution to the activation energy.

Conclusions

Gradient-corrected density functional calculations have been used to compute reaction profiles for the oxidative addition of NH_3 to a variety of unsaturated low-valent transition metal fragments. Strong NH_3 adducts are formed with d^8 CpM(CO) and M(PH_3)$_2$X fragments (M = Rh, Ir; X = Cl, H) from which activation energies for oxidative addition are in the range 20−25 kcal mol^{-1} (M = Rh) and 16−17 kcal mol^{-1} (M = Ir). The overall oxidative addition process is exothermic with all these d^8 fragments but is about 15−20 kcal mol^{-1} more so for the third-row species. NH_3 adducts formed with M(PH_3)$_2$ fragments (M = Pd, Pt) are weak, and activation barriers are high (24 and 30 kcal mol^{-1}, respectively). The overall oxidative addition process is endothermic for both metals. Calculations with M(dpe) fragments show slightly reduced activation barriers and much greater reaction exothermicity compared to the M(PH_3)$_2$ species. NH_3 oxidative addition is computed to be most favorable with the CpIr(CO), Ir(PH_3)$_2$X, and Pt(dpe) fragments, from both the kinetic and thermodynamic points of view. The more favorable thermodynamics for NH_3 oxidative addition in the third-row transition metal systems are a result of stronger M−H and M−NH_2 bond strengths in the products. In saturated species M−H homolytic bond strengths are computed to be up to 26 kcal mol^{-1} stronger than for M−NH_2 bonds. Where N→M π-donation occurs, M−H and M−NH_2 bonds can have similar homolytic bond strengths. The relative insensitivity of the computed activation energies with the CpIr(CO), Ir(PH_3)$_2$X, and Pt(dpe) fragments can be rationalized in terms of the varying role of the transition metal fragments during the oxidative addition process. Thus strong Lewis acids make NH_3 reorientation difficult but generally promote N−H bond activation, while weak Lewis acids allow relatively facile NH_3 reorientation but are generally less efficient at the N−H bond activation step.

Acknowledgment. The support of the EPSRC and Heriot-Watt University is gratefully acknowledged.

Supporting Information Available: Tables of Cartesians coordinates of all optimized structures are available free of charge via the Internet at http://pubs.acs.org.

OM010044W